ACCEPTED MANUSCRIPT

Room Temperature Self- and H_2-Broadened Line Parameters of Carbon Monoxide in the First Overtone Band: Theoretical and Revised Experimental Results

Koorosh Esteki[1,2], Adriana Predoi-Cross[1*], Chad Povey[1], Sergey Ivanov[3], Aziz Ghoufi[4], Franck Thibault[4], Mary Ann H. Smith[5]

[1] Department of Physics and Astronomy, University of Lethbridge, Lethbridge, AB, Canada

[2] Present address: Mechanical and Manufacturing Engineering, Schulich School of Engineering, University of Calgary, Calgary, AB, Canada

[3] Federal Scientific Research Centre "Crystallography and Photonics" of Russian Academy of Sciences (FSRC "Crystallography and Photonics" RAS), Leninsky pr. 59, Moscow, 119333, Russia

[4] Institut de Physique de Rennes, UMR CNRS 6251, Université de Rennes 1, Campus de Beaulieu, F-35042 Rennes, France

[5] Science Directorate, NASA Langley Research Center, Hampton, VA, USA

[*]Corresponding author. Department of Physics and Astronomy, University of Lethbridge, Lethbridge, AB, T1K 3M4 Canada, Tel: 403-329-2697 Fax: 403-329-2057, E-mail: adriana.predoicross@uleth.ca

Accepted manuscript

Abstract

Lorentz self- and H_2-broadened half-width and pressure-induced shift coefficients, line mixing coefficients as well as line center positions and intensities were obtained using a nonlinear least square fitting technique for 48 (P(24) to R(23)) ro-vibrational transitions belonging to the first overtone (2←0) band of $^{12}C^{16}O$ at room temperature. All spectra in the 4146 to 4332 cm^{-1} spectral interval were fitted simultaneously employing four line shape functions: the Voigt, Speed Dependent Voigt, Rautian and Speed Dependent Rautian profiles. The collisional line mixing effect has been observed and investigated as an asymmetry in the analyzed line profiles. A semi-empirical Exponential Power Gap Law method was used to estimate the self- and H_2-broadening coefficients and the collisional line mixing parameters. Additionally, a classical approach was applied to calculate the half-width coefficients of

ACCEPTED MANUSCRIPT

transitions in the 2←0 band for carbon monoxide broadened by H_2 and for pure CO. The classical approach based on a simple computational method, ensures the molecular motion is correctly characterized in 3 dimensions. The calculations used vibrationally independent intermolecular interaction potentials. The variation of CO half-width coefficients with rotational quantum number $J \leq 24$ was computed and compared with measurements. The agreement between the theoretical broadening coefficients is better for pure CO rather than for the CO-H_2 system.

Keywords:
carbon monoxide, CO widths, CO shifts, H_2, hydrogen, infrared spectra, line mixing, spectral line shapes, speed dependence

Accepted manuscript

1. Introduction

Carbon monoxide (CO) has been the subject of numerous investigations in recent decades due to its ability to offer insight into the evolution of galactic and extragalactic astrophysical entities [1]. The presence of CO in Jupiter's atmosphere was first reported in 1975 [2] and CO was later found in the atmospheres of the other giant planets, Saturn [3], Neptune [4, 5], and Uranus [6] and in the atmosphere of Saturn's moon, Titan [7]. The infrared lines of CO corresponding to the first overtone band were discovered in spectra of the predominantly CO_2-rich atmospheres of Venus and Mars [8,9]. Moreover, CO is an attractive candidate for scientists to perform high signal-to-noise laboratory measurements (see, e.g. [10]).

The upcoming missions such as the GEO stationary Coastal and Air Pollution Events (GEO-CAPE), Global Atmospheric Composition Mission (GACM) and Active Sensing of CO_2 absorption over Nights, Days and Seasons (ASCENDS) will map the spectral radiances located in the 2.3 μm region to obtain distributions of concentrations for terrestrial atmospheric CO [11]. Accurate retrievals of atmospheric composition from spectra recorded by remote sensing techniques rely on having access to highly accurate line parameters for both self- and foreign-gas broadening. While considerable progress has been made in improving self- and air-broadened

ACCEPTED MANUSCRIPT

line parameters in the 2←0 band of CO (see Ref. [11]), our present study focuses on self- and H_2-broadening in the same band, and in the following paragraphs we briefly review the previously available measurements.

Self-broadening parameters in the first overtone band of CO have been reported in numerous studies, while H_2-broadened line shapes have been studied less often. The half-width coefficients of self-broadened transitions in the 2←0 and the 3←0 bands of CO have been measured by Plyler *et al.* [12] using a high resolution grating spectrometer for 21 lines in the R-branch over a range of pressures between 1.5 to 4 atm. James *et al.* [13] have published measurements of pressure-broadened widths for 20 transitions in the 2←0 band of CO by hydrogen and nitrogen at 295 K for several pressures in the range of 10 to 35 Torr using a 1-m long gas cell attached to a Jarrel-Ash Ebert spectrometer. Hunt *et al.* [14] have reported the room temperature half width coefficients of 31 self-broadened lines in the first overtone band of CO in the pressure range of 1 to 2 atm with an estimated accuracy of ±3.0% employing a high-resolution Littrow type grating spectrometer at a resolution of 0.045 cm^{-1}.

Bouanich *et al.* [15] have studied the self- and foreign-broadened widths of 22 transitions belonging to the first overtone band of CO perturbed by N_2, H_2, O_2, NO, HCl, and CO_2 at 299 K and pressures ranging from 1 to 5 atm. Bouanich *et al.* [16] also determined the self-broadened half-width coefficients of 22 lines in the P- and R-branches of CO at 298, 198, 131, and 85 K along with their temperature dependences.

Bouanich *et al.* [17] have used a tunable difference frequency laser spectrometer to measure the broadening and shift parameters in the 2←0 band of CO. They measured self-, He-, Kr-, O_2-, and N_2-broadened coefficients for several lines, and compared them with theoretical estimations based upon the semi-classical model by Robert-Bonamy and different interaction potentials.

Pressure broadening, pressure shift, and line mixing parameters of 42 lines of the first overtone band of pure CO and CO broadened by N_2 have been investigated by Predoi-Cross *et al.* [18] using spectra recorded with a Bomem DA8.003 Fourier transform spectrometer at 303 K at various gas sample pressures. The authors have used the Lorentz profile to retrieve spectral line parameters for pure carbon monoxide as well as a Voigt and an empirical line shape model (HC_v) which combines hard collision and speed-dependent Lorentz models to retrieve line parameters. They also compared the line broadening and pressure-shift coefficients with semi-

Accepted manuscript

ACCEPTED MANUSCRIPT

classical computations. The measured line mixing parameters were compared with line mixing computations based upon an empirical energy corrected sudden scaling law.

Zou and Varanasi [19] have published self- and air-broadening coefficients, self- and air-induced shift parameters of the 1←0 and 2←0 bands of carbon monoxide for transitions between the P(24) and R(26) lines. The spectra were recorded at several temperatures ranging from 174 K to room temperature using a Bruker IFS-120HR Fourier transform spectrometer. In addition, they reported line positions and intensities, as well as the temperature dependences of the broadening and shift coefficients for each studied transition.

The line positions, intensities, broadening and pressure-induced shift parameters for pure CO and CO diluted in H_2 belonging to the first overtone band were reported by Devi *et al.* [20] at 297 K for pressures between 3 and 507 Torr using the former Fourier transform spectrometer at the McMath-Pierce Solar Telescope, Kitt Peak National Observatory, AZ. Their measurements cover the 4130 to 4345 cm^{-1} region corresponding to transitions between P(27) and R(27). The authors have studied the vibrational dependence of the self-shift parameters by comparing them with coefficients published in previous spectroscopic works on the fundamental band. Line mixing effects could not be quantified in their data analysis.

Brault *et al.* [21] studied line positions and intensities, self-broadened widths, pressure-induced shifts and line mixing parameters in the (2←0) band of CO for the P(23) to R(23) transitions at temperatures between 297.8 to 301.6 K and pressures from 200 to 600 Torr applying the Voigt and Speed Dependent Voigt (SDV) models. The authors have also calculated the transition dipole moments using the intensity information and compared them with the Herman-Wallis parameters for transitions in this band.

Using a Bruker IFS-120HR Fourier transform spectrometer Sung *et al.* [22] have measured H_2-broadened half-widths and H_2-induced pressure-shift coefficients and determined the temperature dependences for the fundamental (1←0), first overtone (2←0) and second overtone (3←0) bands over a temperature range between 83 and 302 K and pressures from 101.11 to 539.74 Torr.

Since there was considerable disagreement between the H_2-broadened results of Devi *et al*. [20] and those of Ref. [22], pressure-induced shift and half-width coefficients of pure CO and CO-H_2 mixtures were re-measured by Devi *et al.* [23] employing the multispectrum nonlinear least squares method [24] with a new set of H_2-broadened spectra. The authors have analyzed 48

ACCEPTED MANUSCRIPT

transitions between P(24) and R(24) in the 2←0 band of CO at room temperature and pressure range from 3 to 643 Torr using a Voigt profile.

Regalia-Jarlot *et al.* [25] have studied the broadening and pressure-induced shift coefficients of CO diluted by air and H_2 in the 1←0 band as well as self- and H_2-broadened line widths and shifts in the 2←0 band, analysing spectra recorded with a Fourier transform spectrometer operating in stepping mode.

Devi *et al.* [11] have determined self- and air-broadened Lorentz half-width and pressure-induced shift coefficients and their temperature dependences of CO in the first overtone band using spectra recorded over the temperature and pressure ranges of 151.15 to 298 K and pressures of 5.11 to 699.14 Torr, respectively. Retrieving precise line positions and intensities enabled them to determine rovibrational constants (*G, B, D* etc.) employing a multispectrum nonlinear least squares spectrum fitting technique. The authors have reported the speed-dependent line shape parameters along with collisional line mixing coefficients obtained by applying the off-diagonal relaxation matrix element (ORME) formalism to obtain best fit residuals.

Our review of the literature indicates that no studies have been reported for the spectral line parameters of carbon monoxide perturbed by hydrogen in the second overtone band since 2005. In this study, we have re-analyzed the high-resolution spectra of self-broadened CO and CO broadened by hydrogen [20,23] recorded in the first overtone band. We have used four different line shapes in the multispectrum analysis (Voigt, speed dependent Voigt, Rautian, and Rautian with speed dependence) and compared the resulting line shape parameters with results available in the literature. These four models allowed us to investigate the contributions of Dicke narrowing and speed-dependence to the measured line shapes.

Line mixing coefficients have been calculated using the Exponential Power Gap (EPG) law. A classical approach was applied to calculate CO line widths for collisions of pure carbon monoxide and of mixtures of carbon monoxide and hydrogen, both performed using simple interaction potentials.

2. Experimental description

Absorption spectra of high purity research-grade (99.999%) carbon monoxide ($^{12}C^{16}O$) purchased from Matheson Inc. and samples of the same high-purity carbon monoxide mixed with

Accepted manuscript

ACCEPTED MANUSCRIPT

dry, research grade hydrogen in the (2←0) band of CO were recorded at high resolution (0.0052 - 0.0055 cm^{-1}) using the former Fourier transform spectrometer situated on Kitt Peak, AZ. Details regarding the spectra and the data acquisition procedure are given in Refs. [20, 23].

For the convenience of the reader, a brief summary of the experimental details is provided here. Ten pure CO and eight H_2-broadened CO ($CO+H_2$) spectra with different mixing ratios were recorded at room (~297.90-298.20 K) temperature. The experimental setup consisted of a Globar light source at 12 V and CaF_2 beam splitter. The experimental conditions of all the spectra analyzed in this work are given in Table 1. A LN_2-cooled InSb detector was employed in recording the spectra. The signal to noise ratio (S/N) was estimated to be in the 200 to 500 range. The entire spectral region extends between 4146 and 4332 cm^{-1}. Overlaid CO spectra used in the present study are shown in panel (B) of Figure 1. The top panel presents the differences between observed and calculated spectra. The concentrations of the spectra studied in Ref. 20 have been re-calculated using the present line intensities for pure CO and we have entered the revised volume mixing ratios in Table 1.

3. Spectroscopic analysis

For remote sensing applications, the Voigt line shape model (VP) (see Eqs. (2-5) of Ref. [26]) has been used for several decades. The line shape function known as the Speed Dependant Voigt profile (SDV) (see Eq. (11) of Ref. [26]) introduced first by Berman *et al.* [27] and later expanded by Pickett [28] is a weighted summation of Lorentzian profiles according to different absorber speeds and incorporates the dependence of relaxation rates term on the speed of the absorber. The analysis software employed in this study uses the implementation of speed-dependence introduced by Rohart *et al.* (see Eqs. (10) Ref. [26] and references therein).

The Voigt or speed dependent Voigt line shape functions is only satisfactory when it is assumed that the mean-free path of the molecule is much larger than the wavelength of the incident radiation. So, if this condition is not met, and if the memory about coherence with the radiation is preserved after collision, smaller broadening parameters would be expected. This phenomenon is known as the Dicke narrowing effect [29] and has to be taken into account by adopting appropriate model.

The Galatry profile (GP) [29] is used when the molecular collisions are assumed to be soft (i.e., a great number of collisions are needed to yield a noticeable change in velocity, meaning

Accepted manuscript

ACCEPTED MANUSCRIPT

the effect of only one collision is small and can be ignored). The Rautian and Sobel'man line shape formulation (RP) ([30] or Eqs. (5-6) of Ref. [26]) and the one of Nelkin-Ghatak [31] have been introduced to account for hard collisions (i.e., for molecular systems where each collision randomizes the velocity, based upon a Maxwellian distribution [32], and thus the velocity memory is lost [33]). Collisional narrowing was implemented assuming that it can be related to the molecular diffusion.

Practically, the speed dependence of the velocity changing collisions and relaxation rates turn up simultaneously. Ciurylo and Szudy [34] described the collisional broadening applying the classical shift theory by Anderson [35] and the thermal motion of absorbing molecules by the Galatry model and introduced the speed dependent Galatry (SDG) line shape profile. By integrating the speed dependence relaxation rate in Rohart's approximation (see Eqs. (10) Ref. [26] and references therein) in the Rautian and Sobel'man formulation [33], we can obtain the speed dependent Rautian (SDR) profile.

To obtain the self- and air-broadened half-width and pressure-induced shift parameters, the following two equations are needed:

$$\gamma(p,T) = p\left[\gamma^0_{H_2}(p_0,T_0)(1-\chi)\left[\frac{T_0}{T}\right]^{n_1} + \gamma^0_{self}(p_0,T_0)\chi\left[\frac{T_0}{T}\right]^{n_2}\right] \quad (1)$$

$$v(T) = v_0 + p\left[\delta^0_{H_2}(T)(1-\chi) + \delta^0_{self}(T)\chi\right] \quad (2)$$

where δ^0 and $\gamma^0_{H_2}$ represent the retrieved pressure-shift and Lorentzian half-width coefficients (in cm^{-1} atm^{-1}) at the reference pressure (p_0 = 1 atm) and temperature (T_0 = 296 K), respectively. $\gamma(p,T)$ expressed in cm^{-1} is the Lorentzian half-width of the line at the pressure p ($p = p_{CO} + p_{H_2}$) and temperature T. n_1 and n_2 are the temperature dependence exponents of half-width coefficients and χ is the volume mixing ratio of CO in the pressure-broadened spectra.

The transition intensity between each two rovibrational states of any molecule possessing electrical dipole moment for a pure gas can be described by the following expression [36]:

$$S_{ij} = \frac{I_a A_{ij}}{8\pi c v_{ij}^2}\frac{g' e^{-hcE''/(k_B T)}\left(1-e^{-hcv_{ij}/(k_B T)}\right)}{Q(T)} \quad (3)$$

In the equation above, S_{ij} is the weighted spectral line intensity based upon the natural terrestrial isotopologue abundances, I_a (for $^{12}C^{16}O$ is equal to 0.986544), introduced with the unit of (cm^{-1}/ (molecule. cm^{-2})) to describe it as the wavenumber per column density. h is Planck's constant, c is the speed of light, T is the temperature (K) and v_{ij} is the transition wavenumber (cm^{-1}). A_{ij} is

ACCEPTED MANUSCRIPT

the Einstein coefficient in s^{-1}, E'' is the lower state energy (cm^{-1}) and g' is the is the upper state statistical weight which can be estimated by $g = g_\varepsilon g_{rot} = (2J+1)g_s g_i$ (g_ε stands for total degeneracy yielding from the product of vibrational and electronic statistical weight, and g_i and g_s are the state-independent and state-dependent nuclear spin statistical weights, respectively (in the case of carbon monoxide, $g_i = g_s = 1$). Double prime and prime ($''$ and $'$) correspond as usual to the lower and upper states, respectively. $Q(T)$ is the total internal partition function and k_B is the Boltzman constant. Note that equation (3) can only be applied for those molecules that have electrical transition dipole moments.

A dispersion parameter is required to be implemented in the line shape function of interest when a weak asymmetry is observed in the spectral lines that is characteristic to line mixing effects [37]. We least squared fitted the spectral interval (4146-4332 cm^{-1}) corresponding to the entire band, all at once, rather than analyze the transitions one by one, and we used the ORME formalism [38]. The pressure broadening and the pressure shift coefficients come from the real and imaginary parts of the diagonal relaxation matrix elements, as shown in the following expression:

$$W_{kk}^0 = \gamma_k + i\delta_k \tag{4}$$

The off-diagonal elements of the relaxation matrix are labeled W_{lk}^0. These elements cause mixing of the lines *l* and *k*. For a given line interacting with all the other lines, the coefficient which realizes that effect can be represented as follows [37]:

$$Y_k^0(T) = 2\sum_{l\neq k}\frac{d_l}{d_k}\frac{W_{lk}^0}{v_k - v_l}. \tag{5}$$

$Y_k^0(T)$ are the first order, Rosenkranz [37], line mixing coefficients, and this theory works well if the spectral lines are separated well enough. In Eq. (5) d_l and d_k are the dipole moments of the optical transitions, v_l and v_k are the line centers of the transitions at zero pressure. Finally, the off-diagonal matrix elements are approximated by (minus) state-to-state rotational transfer rates (see [33,38] for a review). With the help of the Rosenkranz [37] line profile, the expression for the collisional absorption coefficient is given by:

$$\alpha(v) = \frac{1}{\pi}\sum_l S_l \frac{p\gamma_l^0 + pY_l^0(v - v_0^l - p\delta_l^0)}{(v - v_0^l - p\delta_l^0)^2 + (p\gamma_l^0)^2} \tag{6}$$

Accepted manuscript

ACCEPTED MANUSCRIPT

where " *l"* designates a rovibrational line $\nu_i j_i \rightarrow \nu_f j_f$. In Eq. (6) p is the total pressure, ν_0^l is the line position of the spectral line *l*, Y_l^0, γ_l^0 and δ_l^0 are the line mixing coefficients, half-width at half maximum and pressure induced shift coefficients per atm, respectively.

There are several semi-empirical scaling laws such as the Energy Corrected Sudden (ECS), Exponential Power Gap (EPG) and Modified Exponential Gap Law (MEGL) that can be used to predict the values of the relaxation matrix elements [33,38].

The EPG scaling law makes use of standard collisional transfer rates, $k(\nu_i j_i \rightarrow \nu_i j_i', T)$, between the rotational levels j_i and j_i' belonging to the same vibrational state ν_i. The expression for the collisional transfer rate from lower to a higher rotational level, exploiting the EPG law is given by the following equation [33,38]:

$$k(\nu_i j_i \rightarrow \nu_i j_i', T) = a\left[\frac{\left|\Delta E_{j_i j_i'}\right|}{B_0}\right]^{-b} \exp\left(\frac{-c\left|\Delta E_{j_i j_i'}\right|}{B_0}\right) \quad (7)$$

Here, $\Delta E_{j_i j_i'}$ is the energy difference (in cm^{-1}) between each two rotational levels, B_0 is the rotational constant (in cm^{-1}) corresponding to the ground vibrational state, *a*, *b* and *c* are the adjustable parameters that need to be optimized applying nonlinear least squares technique. The real part of the diagonal element of the relaxation matrix can be approximated as follows (the so called random phase approximation):

$$Re(W_{kk}) = \frac{1}{2}\left\{\sum_{j_i' \neq j_i} k(\nu_i j_i \rightarrow \nu_i j_i', T) + \sum_{j_f' \neq j_f} k\left(\nu_f j_f \rightarrow \nu_f j_f', T\right)\right\} \quad (8)$$

In our approach we have ignored the vibrational dependence of the collisional rates.

4. Theoretical calculations of CO- and H_2-broadening coefficients

In this section, we present the first results of classical trajectory calculations of CO pressure-broadening coefficients for pure CO-CO and mixtures of CO and H_2. A classical trajectory approach to compute the impact line broadening, shift and line mixing coefficients was proposed by R.G. Gordon [39,40] in 1966. The classical approach enables an exact three-dimensional (3D) self-consistent characterization of translational and rotational motion of molecules without fitting for any parameters. This method is simple, visual, and computationally efficient. This classical approach, with applications to a variety of molecular systems [41-53], has been shown to be efficient and constitutes an accurate tool that provides theoretical results that are in much better agreement with benchmark quantum and/or experimental data, when

ACCEPTED MANUSCRIPT

compared with the results of semi-classical formalisms in cases where an accurate and robust *ab initio* based potential energy surface (PES) is used.

In the framework of the classical impact theory, the collisional half-width, γ, and pressure shift, δ, of electric dipole vibration-rotational spectral line are given by [39,40]:

$$\gamma = \frac{n_b \bar{v}}{2\pi c} Re\sigma \qquad \delta = -\frac{n_b \bar{v}}{2\pi c} Im\sigma \qquad \bar{v} = \sqrt{8k_B T/\pi\mu} \tag{9}$$

where the cross sections, σ are as follows

$$\text{for } P\text{- lines } \sigma = \langle v \left\{1 - P_{el} exp[-i(\eta_{vib} + \eta)] \cos^2 \frac{\beta}{2}\right\}\rangle_{b,V,O} \; . \; \bar{v}^{-1} \tag{10}$$

$$\text{for } R\text{- lines } \sigma = \langle v \left\{1 - P_{el} exp[-i(\eta_{vib} - \eta)] \cos^2 \frac{\beta}{2}\right\}\rangle_{b,V,O} \; . \; \bar{v}^{-1}. \tag{11}$$

Here, n_b is number density of perturbing particles; c is the speed of light; μ is the reduced mass of the colliding pair; T is the temperature and k_B is the Boltzmann constant. P_{el} is the probability of a given collision to be elastic (P_{el} is calculated using box-quantization [44]). The average $\langle \ldots \rangle$ is calculated over the impact parameter b, at relative speed v and using the initial orientations (denoted here by O) of the axes $\vec{r}_1$ and $\vec{r}_2$ of both interacting molecules and the directions of their angular velocities, $\vec{\omega}_1$ and $\vec{\omega}_2$. The variable η characterizes the "rotational dephasing" due to collisions and ?? is the angle between the before and after collision orientations of the active molecule's angular momentum ("rotational reorientation"). The values of P_{el}, η and ?? are calculated from the dynamics of each particular collision by the modified method described in [41,50].

The vibrational phase shift, η_{vib}, is defined by [39,40]

$$\eta_{vib} = \hbar^{-1} \int_{coll} (V_u - V_l) dt \tag{12}$$

where, V_l and V_u are the full intermolecular potential energies in the lower and upper vibrational states of the optical transition under consideration and the integral is taken over the collision trajectory. In our present calculations, we neglect this vibrational phase shift since molecules are treated as rigid rotors and we use the simple vibrationally independent PES. Line shift calculations are not performed since line shift is much more sensitive to vibrational dephasing than line width.

All calculations of half-widths of $^{12}C^{16}O$ electric dipole transitions perturbed by H_2 and CO were made for the room temperature (T = 296 K). The classical 3D dynamics (C3D) for collision of two rigid diatomic molecules is characterized by applying 17 first-order Hamilton differential

Accepted manuscript

ACCEPTED MANUSCRIPT

equations within body-fixed frames [44]. Broadening coefficients of CO molecule were calculated by considering perturbing molecules located in the ground vibrational state with J_2 values up to 10 for H_2 and up to 57 for CO, weighted by the nuclear spin (1 for collisions with CO and $(-1)^{J_2+1}+2$ for collisions with H_2) and Boltzmann factors. The initial intermolecular distance was set as R_{max}=15 Å for CO and H_2 mixtures and R_{max}=20 Å for pure CO, to ensure that there will be no interaction between molecules. Other collision parameters (initial relative speed v, impact parameter *b*, initial orientations of molecular axes and vectors of angular momentum) were selected via a Monte Carlo procedure. The sample relative velocities were set to follow a Maxwell distribution with temperature, *T*. Uniform sampling was used to select b^2, the orientations of both molecules in 3D space, and the directions of angular momenta. In order to decrease the computation time in the present Monte Carlo calculations we have implemented an efficient algorithm of *b*-sampling developed by Chapman and Green [54]. The parameters impact parameter of collisions were set to: (0–13) Å for CO-H_2 and (0–19) Å for pure carbon monoxide; and the relative velocities were set to (0.01–3)v_p, where v_p is the most probable relative speed of a given colliding pair.

The bond lengths, *r*, of the molecules and their rotational constants, *B*, were fixed to their values in the ground vibrational level (see Table 2, all parameters are taken from Ref. [55]). The initial rotation frequency ω_1 of CO molecule was determined via its rotational quantum number $J=J_1$ by the rigid rotor formulae based on the so called Langer prescription [39,40,54,56]: $\omega_1 = \frac{2B}{\hbar}J$ for *P*-lines and $\omega_1 = \frac{2B}{\hbar}(J+1)$ for *R*-lines.

Hamilton equations of motion were integrated numerically by employing the Gear method [57] (recommended as a method to solve "stiff" problems) using standard IMSL Math Library routine IVPAG. All numerical calculations were performed within fixed time-grid intervals 1·fs using double precision, 10^{-8} tolerance parameter and a variable step of integration. The RMS error of Monte Carlo averaging was below 1 % for calculated line widths at different T_s and J_s.

In our classical calculations for pure carbon monoxide and for mixtures of carbon monoxide and hydrogen, a simple expression of the PES was used for both systems, namely, the sum of the Tipping-Herman (TH) potential, V_{TH} [58] and electrostatic interactions, V_{el}

$$V = V_{TH} + V_{el} \tag{13}$$

ACCEPTED MANUSCRIPT

The Tipping-Herman potential is defined by a three-term expansion in Legendre polynomials as follows:

$$V_{TH} = V_{TH}(R,\theta_1) = V_{R_0}(R) + V_{R_1}(R)P_1(\cos\theta_1) + V_{R_2}(R)P_2(\cos\theta_1) \quad (14)$$

$$V_{R_0}(R) = 4\varepsilon\left[\left(\frac{\sigma}{R}\right)^{12} - \left(\frac{\sigma}{R}\right)^{6}\right];\ V_{R_1}(R) = 4\varepsilon\left[R_1\left(\frac{\sigma}{R}\right)^{13} - A_1\left(\frac{\sigma}{R}\right)^{7}\right];\ V_{R_2}(R) = 4\varepsilon\left[R_2\left(\frac{\sigma}{R}\right)^{12} - A_2\left(\frac{\sigma}{R}\right)^{6}\right].$$

Here θ_1 is the angle between the axis of CO molecule and the vector of intermolecular center-of-mass separation, $\vec{R}$; $P_1(\cos\theta_1)$ and $P_2(\cos\theta_1)$ are the Legendre polynomials; ε and σ are the Lennard-Jones (LJ) potential parameters. Electrostatic interactions include dipole-dipole, dipole-quadrupole and quadrupole-quadrupole interactions (see, e.g., [59]):

$$V_{el} = V_{el}(R,\theta_1,\theta_2,\varphi_1,\varphi_2) = V_{\mu_1\mu_2} + V_{\mu_1 Q_2} + V_{\mu_2 Q_1} + V_{Q_1 Q_2}, \quad (15)$$

$$V_{\mu_1\mu_2} = -\frac{\mu_1\mu_2}{R^3} f_{\mu_1\mu_2}(\theta_1,\theta_2,\varphi_1,\varphi_2) \quad ; \quad V_{\mu_1 Q_2} = \frac{3}{2}\frac{\mu_1 Q_2}{R^4} f_{\mu_1 Q_2}(\theta_1,\theta_2,\varphi_1,\varphi_2);$$

$$V_{\mu_2 Q_1} = \frac{3}{2}\frac{\mu_2 Q_1}{R^4} f_{\mu_2 Q_1}(\theta_1,\theta_2,\varphi_1,\varphi_2) \quad ; \quad V_{Q_1 Q_2} = \frac{3}{4}\frac{Q_1 Q_2}{R^5} f_{Q_1 Q_2}(\theta_1,\theta_2,\varphi_1,\varphi_2).$$

Here μ_1, μ_2 are the dipole moments and Q_1, Q_2 are the quadrupole moments of the interacting molecules; θ_1, θ_2 and φ_1, φ_2 are usual polar and azimuth angles of molecular axes in the body-fixed coordinate system (note that its z-axis is always directed along the $\vec{R}$ vector). Note also that for CO-H_2 interaction $V_{\mu_1\mu_2} = 0$ since H_2 molecule has no dipole moment. Angular functions for electrostatic interactions are given by [59]:

$$f_{\mu 1\mu 2}(\theta_1,\theta_2,\varphi_1,\varphi_2) = 2\cos\theta_1\cos\theta_2 - \sin\theta_1\sin\theta_2\cos(\varphi_1 - \varphi_2) \quad (16)$$

$$f_{\mu_1 Q_2}(\theta_1,\theta_2,\varphi_1,\varphi_2) = \cos\theta_1(3\cos^2\theta_2 - 1) - 2\sin\theta_1\sin\theta_2\cos\theta_2\cos(\varphi_1 - \varphi_2)$$

$$f_{\mu_2 Q_1}(\theta_1,\theta_2,\varphi_1,\varphi_2) = \cos\theta_2(3\cos^2\theta_1 - 1) - 2\sin\theta_2\sin\theta_1\cos\theta_1\cos(\varphi_2 - \varphi_1)$$

$$f_{Q_1 Q_2}(\theta_1,\theta_2,\varphi_1,\varphi_2) = 1 - 5(\cos^2\theta_1 + \cos^2\theta_2 + 3\cos^2\theta_1\cos^2\theta_2) + 2[\sin\theta_1\sin\theta_2\cos(\varphi_1 - \varphi_2) - 4\cos\theta_1\cos\theta_2]^2$$

In above equations we set $R_1 = 2A_1 = 12d_{mc}/\sigma$, $R_2 = A_2 = \rho$, where d_{mc} is the separation of the CO center-of-mass and the center-of-charge and ρ is the reduced polarizability anisotropy of CO molecule.

The values of dipole and quadrupole moments of CO and H_2 molecules used in the calculations are given in Table 2. In the present classical calculations we did not fit the parameters of the Tipping-Herman interaction potential to experimental data (as was done in

ACCEPTED MANUSCRIPT

previous papers [18,55] using the semi-classical Robert-Bonamy method) but tried to use unadjusted (theoretical or measured) ones. We used three different sources for LJ interaction parameters, ε and σ, (see Table 3). For reduced polarizability anisotropy of CO molecule, $\rho = (\alpha_{\parallel} - \alpha_{\perp})/(\alpha_{\parallel} + 2\alpha_{\perp})$, where $\alpha_{\parallel}$ and $\alpha_{\perp}$ are the polarizabilities of CO molecule along the bond and perpendicular to the bond, respectively,, we used two very different data: ρ = 0.16667 [59] and ρ = 0.089 [55, 60, 61].

For the separation of the CO center-of-mass and center-of-charge, we used fixed value d_{mc} = 0.21 Å [62]. Then $R_1 = 12d_{mc}/\sigma$, $A_1 = R_1/2$, $R_1 = A_2 \approx \rho \equiv (\alpha_{\parallel} - \alpha_{\perp})/(\alpha_{\parallel} + 2\alpha_{\perp})$. As for LJ interaction parameters, ε and σ, we took their values from the books [59] and [63] and from the article [55] (see Table 3).

5. Results and data analysis

5.1 Narrowing coefficients

In order to account for the narrowing effects for both hard and soft collisional cases we have first determined the dynamical friction parameter (β_{diff} in cm^{-1}/atm) which is given by the following equation for the frequency of elastic velocity-changing collisions:

$$\beta_{diff} = \frac{k_B T}{2\pi c M D} . \quad (17)$$

Here, k_B is the Boltzmann constant, T is the temperature (K), D is the mass diffusion constant (m^2/s), M is the mass of the absorber (kg) and c is the speed of light (cm/s).

The H_2 molecule was modeled by means of a single united atom force field [64] while CO was described as a three electrostatic sites model [65]. Intermolecular interactions were described by combining electrostatic and van der Waals interactions. For both interactions, a cutoff of 12 Å was used. Electrostatic contribution was computed by using the Ewald sum with a convergence parameter of 0.36 $Å^{-1}$ while the van der Waals interactions were modeled from Lennard-Jones (LJ) potential. Crossed LJs interactions were evaluated from the Lorentz-Berthelot mixing rule. For CO-H_2 mixtures, eight volume fractions, corresponding to the experimental spectra, were investigated (Table 4). Lengths of box are $L_z = L_y = L_x$ = 344 Å. Molecular dynamics (MD) simulations were carried out from DLPOLY software [66]. Time-step of 1 fs was used. The acquisition phase corresponds to 10 ns after an equilibration period of 5 ns. MD runs were performed in the NVT statistical ensemble where N is the number of particles, T

Accepted manuscript

ACCEPTED MANUSCRIPT

the temperature, V the volume of the simulation box. Temperature and pressure are 300 K and 1 bar respectively. In canonical ensemble temperature was kept constant by means of Nosé-Hoover algorithm [67] such that the relaxation time of the thermostat was 0.5 fs. Integration of the motion equations was performed by using the velocity Verlet algorithm [68]. Mean Square Displacement (MSD) was computed by using the following correlation expression:

$$MSD(t) = \langle \frac{1}{N} \sum_{i=1}^{N} ((\vec{r_i}(t) - \vec{r_i}(0))^2 \rangle \quad (18)$$

where $\vec{r_i}(t)$ denotes the position of a particle i at time t and N the number of particles. In an isotropic medium, self-diffusion coefficient (D_s) in an isotropic phase was computed from MSD

$$D_S = \frac{1}{6} \lim_{t \to \infty} \frac{MSD}{t} \quad . \quad (19)$$

The Maxwell-Stephan diffusion was managed by means of the model of Darken [69]:

$$D_{12} = x_1 D_1 + x_2 D_2 \quad (20)$$

where x_1 and x_2 are the molar fraction of both 1 and 2 components and D_1 and D_2 are the self-diffusion constants of 1 and 2. Indeed, it has been shown that the model of Darken is in quantitative agreement with the expression for the binary Maxwell-Stefan diffusion coefficient [70,71]. Calculated self and binary diffusion coefficients as well as related dynamical friction coefficients are gathered in Table 4. Ultimately, the latter coefficients were directly used in our line shape analysis to account for the Dicke narrowing regime in RP and SDR models.

5.2 Fits of the experimental spectra

The pressure broadening, pressure shift and line mixing parameters as well as the line positions and intensities for both pure carbon monoxide and carbon monoxide perturbed by hydrogen were determined applying the nonlinear least square multispectrum nonlinear least squares technique described in Ref. [24] to fit all the spectra simultaneously to noise level. Four line shape models as defined in Section 3 were employed to retrieve the required sets of line parameters. All initial values for line parameters for the pure gas were taken from the HITRAN2012 database [72]. In the case of CO-H_2, all values of H_2 broadened widths and line shifts were taken from the GEISA database [73]. We did not use the values from the study in Ref. [11] as initial guesses because we did not want to bias the fit towards those results.

The multispectrum software [24] allows users to fit all the spectra simultaneously to the noise level. In retrieving the line broadening coefficients, we tried to float all the experimental

Accepted manuscript

ACCEPTED MANUSCRIPT

values reported in this work. A list of all adjustable parameters for the EPG scaling law is given in the Table 5. These coefficients have been computed based upon the retrieved Voigt profile results. Since the line mixing coefficients should not depend of the line shape model used, we calculated them only using the line parameters retrieved with the Voigt profile.

All line parameters retrieved experimentally using the VP, SDV, RP and SDR line shape functions are listed in Tables 6-10. The errors listed in parentheses correspond to one standard deviation of the fit. The intensities and line positions of present work were used to obtain Einstein A coefficients applying Eq. (3). Comparisons of retrieved and calculated broadening at half-width at half-maximum (HWHM), collisional pressure shift as well as line mixing values are plotted in Figures 2 to 8.

Fig. 2(A) shows a nearly the same average difference of 0.000785 cm^{-1} between the newly retrieved line positions and those stored in the HITRAN or GEISA databases. Fig. 2(B) shows that our retrieved line intensities match better the ones in HITRAN, with average ratios of 1.009 (Voigt) and 1.010 (SD-Voigt). The agreement with the intensities available in the GEISA database is worse with average values of 0.972 (Voigt) and 0.974 (SD-Voigt). The plots for uncertainties in line positions (Fig. 2 (C)) and in line intensities (Fig. 2 (D)) show that the parameters are determined with lower uncertainties when we use the SD-Voigt profile.

Panel (A) of Figure 3 shows that our pure carbon monoxide line broadening coefficients retrieved with the SD-Voigt model are in better with the results from Refs. [11], as compared with the results from Ref. [21]. For the results obtained using the Voigt profile, we have very good agreement with the results in Ref. [18]. Our measured shifts plotted in Figure 3 (A) determined using the Voigt or SD-Voigt models with inclusion of line mixing agree very well with the results obtained through the same type of fit, i.e. Ref. [18] for Voigt results and both Refs. [11,21] for SD-Voigt results, respectively. Panel (B) of Figure 3 shows that the speed-dependent profiles provide slightly higher broadening coefficients than the Voigt or Rautian profiles. The differences between the sets of broadening coefficients obtained with the four profiles are small, but noticeable and are fairly consistent over the range of m values.

The results presented in Fig. 5 for H_2-broadening show a good agreement for $|m|<14$ with both sets of previous results. The scatter in our results for values $|m|>14$ and the departures from the two previous sets [22,23] are attributed to the fact that our set of spectra was not optimal for retrievals of H_2-broadening coefficients at high |m| values. Also, the fact that unlike done in Ref.

ACCEPTED MANUSCRIPT

[23], we have not used a constrained analysis method which is known to remove the scatter in broadening coefficients. The H_2-pressure induced line shifts presented in Figure 6 do not agree very well with previous studies which is not surprising since we have retrieved also H_2-line mixing parameters and the two sets of parameters are known to be highly correlated.

The line mixing coefficients are difficult to retrieve accurately from experimental spectra. Our retrieved values for CO-broadened line mixing coefficients presented in Fig. 7 (A) agree well at medium |m| values with previous measurements and show more scatter at both low and high |m| values where the transitions are weaker. Dicke narrowing, speed-dependence and line mixing, all lead to an effective line narrowing, so these three parameters are all correlated. It is possible that our method of introducing the narrowing parameter based on calculated diffusion constants leads to a underestimation of this parameter. Hence, the experimental values obtained by us for the line mixing coefficients are a bit overestimated. For both CO- and H_2-broadened line mixing coefficients, the best agreement is observed with the semi-empirical results calculated with the Exponential Power Gap law.

In Fig. 8 we present our measured results for speed dependence parameters obtained for pure CO (panel (A)) and for the CO-H_2 system (panel (B)). One striking observation that has to be verified experimentally using new spectra is the very small size of speed-dependence parameters for the CO-H_2 system. As discussed by Kochanov [74], the speed-dependence coefficients are not expected to have a visible J-dependence. The strong J-dependence observed both in the speed-dependence results of Devi *et al.* [11] and in our retrieved speed dependence coefficients is due to the fact that both Dicke narrowing and the speed-dependence effect introduce a narrowing of the lines [74,75], hence making the narrowing and speed-dependence coefficients to be highly correlated. Since in our study we have fixed the narrowing parameter, its J-dependence is neglected and it may have resurfaced in the retrieved speed-dependence coefficients. We have calculated the speed-dependence parameters according to the expressions of Kochanov [75] and we have obtained best agreement with our experimental values for a value of q = 5 in the expression of effective potential $V \sim r^{-q}$, a fact that can be attributed to the contributions from the Van der Waals and quadrupole-quadrupole terms in the interaction potentials.

5.3 Classical calculations of widths and comparisons with experimental data

Accepted manuscript

ACCEPTED MANUSCRIPT

The results of classical calculations of CO line broadening coefficients are shown in Figures 9-14. First of all, we have ascertained that the values of b_{max} (maximum impact parameter) which we used are sufficiently large to provide converged results for the line widths. Fig. 9 and Table 11 represent the broadening convergence with increasing b_{max}. We have checked the validity of the approximation by performing calculations only at the mean thermal velocity (MThV), thus avoiding a thermal average over speeds. This assumption is widely used in line broadening and shift calculations since it greatly reduces CPU time. In this approximation, the initial relative speed, v, in all collisions is fixed to its mean arithmetic speed (see Eq. (9)). The results are presented in Fig. 10 and gathered in Table 12. It is seen that for pure CO this assumption works quite well but for mixtures of CO and H_2 there are some small problems (non-physical behavior of *J*-dependence). So, in all our further calculations we decided (for reliability) to refuse MThV approximation and use Maxwell-Boltzmann speed averaging.

It is known that in molecular collisions sometimes the so called quasi-bound complexes (see, e.g. [53]) arise which may influence the spectral line shape. Special additional calculations showed, however, that their influence on CO line broadening in our cases is negligible. At least, it is so when the Tipping-Herman + electrostatic PES is used.

The comparison of theoretical results with experimental data for self-perturbed CO and CO perturbed by H_2 is shown respectively in Fig. 11 and Fig. 12. Note that calculated pressure broadening coefficients in P- and R- branches are identical for the same |m| values. For self-perturbed CO, the theoretical broadening coefficients were calculated using three different sets of potential parameters (see curves 1–3 in Fig. 11). Classical results for both systems and different potentials used are gathered in Table 13. As one can see there is practically no difference between theoretical results obtained with these different potential parameters. The theoretical and experimental results for the self- and H_2-broadened CO systems were in satisfactory agreement. The magnitudes of maximum and mean relative errors are 16% and 8% for pure CO and 31% and 15% for mixtures of CO and H_2. Note that these values of errors are derived from the comparison of data for R- lines. In this estimation, we used theoretical data with the set of potential parameters designated in Fig. 9.

In Fig. 13 and Fig. 14 we analyzed the contributions of different parts of the interaction potential into the CO pressure broadening coefficients. It is clear from these figures that in both the self- and the H_2-perturbed carbon monoxide cases, the main contributions come, firstly, from

ACCEPTED MANUSCRIPT

the Tipping-Herman (TH) part of the potential and, secondly, from the quadrupole-quadrupole interactions. As for dipole-dipole (dd) and dipole-quadrupole (dQ) interactions, they are very weak and may be neglected and this corroborates the results of Ref. [60]. Table 14 summarizes these results.

The main problem in present classical trajectory calculations relates to the line shifts, more precisely, with accounting for vibrational dephasing, η_{vib} arising from the variation of the PES with the vibrational quantum numbers relevant to the optical transition. In a previous article [55] this variation was taken into account somewhat crudely using fitting parameters for long-range interactions. It was the necessity of that time. Meanwhile, line shift is very sensitive to vibrational dephasing and more delicate methods and PESs should be applied.

There is no such problems with CO line broadening since line-widths only slightly depend on band (they are nearly the same for 1←0, 2←0 and 3←0 bands, see Fig. 2 and 3 of Ref. [55]). So, in this work, both molecules were treated as rigid rotors in calculations of widths (namely, widths are the same for all vibrational bands involving quite low vibrational numbers owing to the CO triple bound).

6. Conclusion and directions for future work

We have reported experimentally measured and theoretical line parameters for transitions in the first overtone (2←0) band of $^{12}C^{16}O$ at the ambient temperature (~298 K) to determine the pressure broadening coefficients for 48 (P(24) to R(23)) rovibrational transitions. Applying a nonlinear least square technique (Labfit software, [24]), all the analyzed spectra were fitted simultaneously to the noise level. Our results agreed well with previous results as mentioned before. Note that there are many experimental studies of carbon monoxide in the first overtone band, and for this reason only a few selected studies have been plotted and compared in the present work. Pressure-broadened half-width coefficients of CO self-perturbed and perturbed by H_2 and collisional line mixing coefficients generated using the EPG scaling law are in good agreement with the experimental values.

Additionally, we present the first results of calculations of self- and H_2-broadened width coefficients of CO using classical impact theory. For a start, we applied very simple interaction PESs which were used in previous works on these molecular systems using the semi-classical Robert and Bonamy approach. However, in our present calculations we did not adjust potential

Accepted manuscript

ACCEPTED MANUSCRIPT

energy parameters but used theoretical (or measured) ones. In spite of the simplicity of the PESs, we obtained quite good results for half-widths, especially for pure CO. It is important to include vibrational state dependence into intermolecular interaction surfaces. It would be the best of all to have robust and up-to-date PESs decomposed into series of bi-spherical harmonics separately for different vibrational states of the CO molecule. After this a reliable classical calculations of line broadening, shift and kinetic parameters (Dicke narrowing, etc.) are straightforward. This study is a step forward towards obtaining information on the narrowing, speed dependence and line mixing parameters that may be needed in the future if databases implement the Hartmann-Tran model recommended by IUPAC [76].

In the future we intend to extend our study using spectra recorded over a large range of pressures and temperatures, to enable us to determine the temperature dependence of line parameters for the CO-CO and CO-H_2 systems. If possible, we would like to test line shape models such as the ones given in Refs. [77-82] that can be used over a range of pressures and include speed dependent effects and line narrowing or line mixing.

Accepted manuscript

Acknowledgments

This work was carried out at the University of Lethbridge funded through the Natural Sciences and Engineering Research Council of Canada and supported by the Discovery and CREATE grant programs. The research performed at the College of William and Mary, Connecticut College and NASA Langley Research Center was supported under contracts and cooperative agreements with the National Aeronautics and Space Administration. We are thankful to Dr. D. Chris Benner at the College of William and Mary for his permission of using multispectrum fitting software, LABFIT, to carry out the data analysis. We thank Mr. Hossein Naseri for his contributions to the early stage of the analysis.

References

[1] Dickman RL, Snell RL, Schloerb FP. Carbon monoxide as an extragalactic mass tracer. APJ 1986;309(1):326-0. doi:10.1086/164604.

ACCEPTED MANUSCRIPT

[2] Beer R. Detection of carbon monoxide in Jupiter. APJ 1975;200(3):L167-9. doi:10.1086/181923.

[3] Noll KS, Knacke RF, Geballe TR, Tokunaga AT. Detection of carbon monoxide in Saturn. APJ 1986;309(2):L91-4. doi:10.1086/184768.

[4] Rosenqvist J, Lellouch E, Romani PN, Paubert G, Encrenaz T. Millimeter-wave observations of Saturn, Uranus, and Neptune - CO and HCN on Neptune. APJ 1992;392(2):L99-2. doi:10.1086/186435.

[5] Marten A, Gautier D, Owen T, Sanders DB, Matthews HE, Atreya SK, Tilanus RPJ, Deane JR. First observations of CO and HCN on Neptune and Uranus at millimeter wavelengths and the implications for atmospheric chemistry. APJ 1993;406(1):285-97. doi:10.1086/172440.

[6] Encrenaz T, Lellouch E, Art PD, Feuchtgruber H, Orton GS, Atreya SK. First detection of CO in Uranus. A&A, 2004;413(2):L5-9. doi: 10.1051/0004-6361:20034637.

[7] Lutz BL, De Bergh C, Owen T. Titan: Discovery of carbon monoxide in its atmosphere. Science 1983:220(4604)1374-5. doi:10.1126/science.220.4604.1374.

[8] Gray Young LD, Young AT. Interpretation of high-resolution spectra of Mars: IV. New calculations of the CO abundance. Icarus 1977:30(1):75-9. doi:10.1016/0019-1035(77)90122-1.

[9] Connes P, Connes J, Kaplan L D, Benedict WS. Carbon monoxide in the Venus atmosphere APJ, 1968;152(3P1):731-4. doi:10.1086/149590.

[10] Seleznev AF, Fedoseev GV, Koshelev MA, Tretyakov MY. Shape of collision-broadened lines of carbon monoxide, J. Quant. Spectrosc. Radiat. Transfer 2015;161:171-9. doi:10.1016/j.jqsrt.2015.04.011.

[11] Devi VM, Benner DC, Smith MAH, Mantz AW, Sung K, Brown LR, Predoi-Cross A. Spectral line parameters including temperature dependences of self- and air-broadening in the 2←0 band of CO at 2.3 μm. J. Quant. Spectrosc. Radiat. Transfer 2012;113:1013-33. doi:10.1016/j.jqsrt.2012.02.010.

[12] Plyler EK, Thibault RJ. Self-broadening of carbon monoxide in the 2 ν and 3 ν bands. J. Re. Natl. Stand. Sec. A 1963;67A(3):229-1. doi:10.6028/jres.067A.022

[13] James TC, Plyler EK. Linewidths in the 2–0 band of carbon monoxide broadened by nitrogen and hydrogen. J. Chem. Phys. 1964;40:221-3. doi:10.1063/1.1724866.

[14] Hunt RH, Toth RA, Plyler EK. High-resolution determination of the widths of self-broadened lines of carbon monoxide. J. Chem. Phys. 1968 ;49 :3909-2. doi:10.1063/1.1670699.

Accepted manuscript

ACCEPTED MANUSCRIPT

[15] Bouanich JP, Brodbeck C. Mesure des largeurs et des deplacements des raies de la bande 0 → 2 de CO autoperturbé et perturbé par N_2, O_2, H_2, HCl, NO et CO_2. J. Quant. Spectrosc. Radiat. Transfer 1973;13(1):1-7. doi:10.1016/0022-4073(73)90095-2.

[16] Bouanich J-P. On the temperature dependence of self-broadening in the first overtone band of CO. J. Quant. Spectrosc. Radiat. Transfer 1984;31 (6):561-7. doi: 10.1016/0022-4073(84)90061-X.

[17] Bouanich J-P, Bermejo D, Domenech JL, Martinez RZ, Santos J. Pressure-induced lineshifts in the 2 ← 0 band of CO self-perturbed and perturbed by He, Kr, O_2, and N_2. J. Mol. Spectrosc. 1996;179(1):22-1. doi:10.1006/jmsp.1996.0180.

[18] Predoi-Cross A, Bouanich J-P, Benner DC, May AD, Drummond JR. Broadening, shifting, and line asymmetries in the 2←0 band of CO and CO–N_2: experimental results and theoretical calculations. J. Chem. Phys. 2000;113(1):158-68. doi: http://dx.doi.org/10.1063/1.481783.

[19] Zou Q, Varanasi P. New laboratory data on the spectral line parameters in the 1-0 and 2-0 bands of $^{12}C^{16}O$ relevant to atmospheric remote sensing. J. Quant. Spectrosc. Radiat. Transfer 2002;75(1):63-92. doi:10.1016/S0022-4073(02)00007-9.

[20] Devi VM, Benner DC, Smith MAH, Rinsland CP, Mantz AW. Determination of self- and H_2-broadening and shift coefficients in the 2-0 band of $^{12}C^{16}O$ using a multispectrum fitting procedure. J. Quant. Spectrosc. Radiat. Transfer 2002;75(4):455-71. doi:10.1016/S0022-4073(02)00023-7.

[21] Brault JW, Brown LR, Chackerian CJr, Freedman R, Predoi-Cross A, Pine AS. Self-broadened $^{12}C^{16}O$ line shapes in the ν=2←0 band. J. Mol. Spectrosc., 2003:222(2):220-39. doi:10.1016/j.jms.2003.07.002.

[22] Sung K, Varanasi P. Hydrogen-broadened half-widths and hydrogen-induced line shifts of $^{12}C^{16}O$ relevant to the Jovian atmospheric spectra. J. Quant. Spectrosc. Radiat. Transfer 2004;85 (2):165-82. doi:10.1016/S0022-4073(03)00202-4.

[23] Devi VM, Predoi-Cross A, Benner DC, Smith MAH, Rinsland CP, Mantz AW, Self- and H_2-broadened width and shift coefficients in the 2 ← 0 band of $^{12}C^{16}O$: revisited. J. Mol. Spectrosc. 2004;228(2):580-92. doi:10.1016/j.jms.2004.05.006.

[24] Benner DC, Rinsland CP, Devi VM, Smith MAH, Atkins D. A multispectrum nonlinear least squares fitting technique. J. Quant. Spectrosc. Radiat. Transfer 1995;53(6):705-21. doi:10.1016/0022-4073(95)00015-D.

Accepted manuscript

ACCEPTED MANUSCRIPT

[25] Régalia-Jarlot L, Thomas X, Von der Heyden P, Barbe A. Pressure-broadened line widths and pressure-induced line shifts coefficients of the (1-0) and (2-0) bands of $^{12}C^{16}O$, J. Quant. Spectrosc. Radiat. Transfer 2005;91(2):121-31. doi:10.1016/j.jqsrt.2004.05.042.

[26] Hashemi R, Rozario H, Povey , Predoi-Cross A. Line-shape models testing on six acetylene transitions in the $\nu_1+\nu_3$ band broadened by N_2. J Quant Spectrosc Radiat Transfer 2014;140:58-66. doi: 10.1016/j.jqsrt.2014.02.013.

[27] Berman PR. Speed-dependent collisional width and shift parameters in spectral line profiles. J Quant Spectrosc Radiat Transfer 1972;12(9):1331-42. doi:10.1016/0022-4073(72)90189-6.

[28] Pickett HM. Effects of velocity averaging on the shapes of absorption lines. J. Chem. Phys. 1980;73(12):6090-4. doi: http://dx.doi.org/10.1063/1.440145.

[29] Galatry L. Simultaneous effect of Doppler and foreign gas broadening on spectral lines. Phys. Rev. 1961;122(4):1218-23. doi:10.1103/PhysRev.122.1218.

[30] Rautian SG, Sobel'man II. The effect of collisions on the Doppler broadening of spectral lines. Sov. Phys. Uspekhi 1967;9(5):701-16. doi:10.1070/pu1967v009n05abeh003212.

[31] Nelkin M, Ghatak A. Simple binary collision model for Van Hove's $G_s(r, t)$. Phys. Rev. 1964;135(1A):A4-9. doi:10.1103/PhysRev.135.A4.

[32] De Vizia MD, Rohart F, Castrillo A, Fasci E, Moretti L, Gianfrani L. Speed-dependent effects in the near-infrared spectrum of self-colliding $H_2{}^{18}O$ molecules. Phys. Rev. A 2011;83(5):052506-1-8. doi: https://doi.org/10.1103/PhysRevA.83.052506.

[33] Hartmann JM, Boulet C, Robert D. Collisional Effects on Molecular Spectra. Elsevier Science, United Kingdom, 2008. doi: 454000054,12,1.

[34] Ciuryło R, Szudy J. Speed-dependent pressure broadening and shift in the soft collision approximation. J. Quant. Spectrosc. Radiat. Transfer 1997;57(3):411-23. doi:10.1016/S0022-4073(96)00078-7.

[35] Anderson PW. A method of synthesis of the statistical and impact theories of pressure broadening. Phys. Rev. 1952;86 (5) 809-9. doi:10.1103/PhysRev.86.809.

[36] Šimečková M, Jacquemart D, Rothman LS, Gamache RR, Goldman A. Einstein A-coefficients and statistical weights for molecular absorption transitions in the HITRAN database. J. Quant. Spectrosc. Radiat. Transfer 2006;98(1)130-55. doi:10.1016/j.jqsrt.2005.07.003.

Accepted manuscript

ACCEPTED MANUSCRIPT

[37] Rosenkranz P. Shape of the 5 mm oxygen band in the atmosphere. IEEE Trans. Antennas. Propag. 1975;AP23(4)498-6. doi:10.1109/TAP.1975.1141119.

[38] Levy A, Lacome N, Chackerian CJr. Spectroscopy of the Earth's atmosphere and of the interstellar medium. In: Rao KN, editor, New York: Academic Press; 1992.

[39] Gordon RG. Theory of the width and shift of molecular spectral lines in gases. J. Chem. Phys. 1966; 44(8):3083-9. doi:10.1063/1.1727183.

[40] Gordon RG. Semiclassical theory of spectra and relaxation in molecular gases. J. Chem. Phys. 1966;45(5):1649-5. doi:10.1063/1.1727808.

[41] Buldyreva J, Ivanov SV, Nguyen L. Collisional line broadening in the atmosphere of light particles: problems and solutions in the framework of semiclassical treatment. J. Raman Spectrosc. 2005;36(2):148-2. doi:10.1002/jrs.1283.

[42] Ivanov SV, Nguyen L, Buldyreva J. Comparative analysis of purely classical and semiclassical approaches to collision line broadening of polyatomic molecules: I. C_2H_2–Ar case. J. Mol. Spectrosc. 2005;233(1):60-7. doi:10.1016/j.jms.2005.05.014.

[43] Nguyen L, Ivanov SV, Buzykin OG, Buldyreva J. Comparative analysis of purely classical and semiclassical approaches to collision line broadening of polyatomic molecules: II. C_2H_2–He case. J. Mol. Spectrosc. 2006;239(1):101-7. doi: 10.1016/j.jms.2006.05.020.

[44] Ivanov SV, Buzykin OG. Classical calculation of self-broadening in N_2 Raman spectra. Mol. Phys. 2008;106(9-10):1291-02. doi: http://dx.doi.org/10.1080/00268970802270034.

[45] Ivanov SV, Buzykin OG. On the accuracy of classical, semiclassical and quantum methods in collision line broadening calculations: comparative analysis for C_2H_2–Ar, He systems. J. Quant. Spectrosc. Radiat. Transfer 2010;111(15) 2341-53. doi: 10.1016/j.jqsrt.2010.04.031.

[46] Thibault F, Ivanov SV, Buzykin OG, Gomez L, Dhyne M, Joubert P, Lepere M. Comparison of classical, semiclassical and quantum methods in hydrogen broadening of acetylene lines. J. Quant. Spectrosc. Radiat. Transfer 2011;112(9)1429-37. doi:10.1016/j.jqsrt.2011.02.011.

[47] Gomez L, Ivanov SV, Buzykin OG, Thibault F. Comparison of quantum, semiclassical and classical methods in hydrogen broadening of nitrogen lines. J. Quant. Spectrosc. Radiat. Transfer 2011;112(12):1942-9. doi: 10.1016/j.jqsrt.2011.04.005.

Accepted manuscript

ACCEPTED MANUSCRIPT

[48] Thibault F, Gomez L, Ivanov SV, Buzykin OG, Boulet C. Comparison of quantum, semi-classical and classical methods in the calculation of nitrogen self-broadened linewidths. J. Quant. Spectrosc. Radiat. Transfer 2012;113(15):1887-97. doi:10.1016/j.jqsrt.2012.06.003.

[49] Povey C, Guillorel-Obregon M, Predoi-Cross A, Ivanov SV, Buzykin OG, Thibault F. Low pressure line shape study of nitrogen-perturbed acetylene transitions in the $\nu_1 + \nu_3$ band over a range of temperatures. Can. J. Phys. 2013;91(11):896-5. doi:10.1139/cjp-2013-0031.

[50] Ivanov SV, Buzykin OG. Precision considerations of classical and semiclassical methods used in collision line broadening calculations: different linear molecules perturbed by argon. J. Quant. Spectrosc. Radiat. Transfer 2013;119:84-94. doi:10.1016/j.jqsrt.2012.12.021.

[51] Thibault F, Martínez RZ, Bermejo D, Ivanov SV, Buzykin OG, Ma Q. An experimental and theoretical study of nitrogen-broadened acetylene lines. J. Quant. Spectrosc. Radiat. Transfer 2014;142:17-4. doi: http://dx.doi.org/10.1016/j.jqsrt.2014.03.009.

[52] Ivanov SV, Boulet C, Buzykin OG, Thibault F. Line mixing effects in isotropic Raman spectra of pure N_2: a classical trajectory study. J. Chem. Phys., 2014;141(18):184306. doi: 10.1063/1.4901084.

[53] Ivanov SV. Quasi-bound complexes in collisions of different linear molecules: Classical trajectory study of their manifestations in rotational relaxation and spectral line broadening. J. Quant. Spectrosc. Radiat. Transfer 2016;177:269-82. doi: 10.1016/j.jqsrt.2016.01.034.

[54] Chapman S, Green S. Rotational excitation of linear molecules by collisions with atoms: Comparison of classical and quantum methods. J. Chem. Phys. 1977;67(5):2317-31. doi: 10.1063/1.435067.

[55] Bouanich J-P, Predoi-Cross A. Theoretical calculations for line-broadening and pressure-shifting in the fundamental and first two overtone bands of CO–H_2. J. Mol. Spectrosc. 2005;742 (1-3):183-0. doi:10.1016/j.molstruc.2005.01.004.

[56] Langer RE. On the connection formulas and the solutions of the wave equation. Phys. Rev. 1937;51(8):669-6. doi: 10.1103/PhysRev.51.669.

[57] Gear CW. Numerical initial value problems in ordinary differential equations. New Jersey: Prentice Hall ; 1971.

[58] Tipping RH, Herman RM. Impact theory for the noble gas pressure-induced HCl vibration-rotation and pure rotation line widths – I. J. Quant. Spectrosc. Radiat. Transfer 1970;10(8):881-96. doi: http://dx.doi.org/10.1016/0022-4073(70):90031-2.

Accepted manuscript

ACCEPTED MANUSCRIPT

[59] Hirschfelder JO, Curtiss CF, Bird RB. Molecular theory of gases and liquids. New York: Wiley and Sons; 1954.

[60] Predoi-Cross A, Bouanich JP, Benner DC, May AD, Drummond JR. Broadening, shifting, and line asymmetries in the 2←0 band of CO and CO–N_2: Experimental results and theoretical calculations. J. Chem. Phys. 2000;113(1):158–68. doi: 10.1063/1.1738101.

[61] Gray CG, Gubbins KE. Theory of molecular fluids. New York: Oxford University Press: 1984.

[62] Friedmann H. The quantum mechanical distribution function of molecular systems: translational and rotational motions. In: Adv. Chem. Phys. John: Wiley & Sons Inc.; 2007, pp. 225-302.

[63] Poling BE, Prausnitz JM, O'Connell JP. The properties of gases and liquids. In: 5th ed., New York: McGraw-Hill; 2001. doi: 10.1039/b517931a

[64] Frost H, Düren T, Snurr RQ. Effects of surface area, free volume, and heat of adsorption on hydrogen uptake in metal−organic frameworks. J. Phys. Chem. B 2006;110(19):9565-0. doi: 10.1021/jp060433 .

[65] Martín-Calvo A, Lahoz-Martín FD, Calero S. Understanding carbon monoxide capture using metal–organic frameworks. J. Phys. Chem. C, 2012;116(11):6655-3. doi: 10.1021/jp211563e.

[66] Todorov IT, Smith W, Trachenko K, Dove MT. DL_POLY_3: new dimensions in molecular dynamics simulations via massive parallelism. J. Mater. Chem. 2006; 16(20) 1911-8 (2006).

[67] Nosé S. A unified formulation of the constant temperature molecular dynamics methods. J. Chem. Phys. 1984;81(1):511-9. doi: 10.1063/1.447334

[68] Allen MP, Tildesley DJ. Computer Simulation of Liquids. United States: Oxford University Press; 1987.

[69] Darken L. Diffusion, mobility and their interrelation through free energy in binary metallic systems. Trans. AIME, 1948;175:184-01. doi:

[70] Fernández GA, Vrabec J, Hasse H. Self diffusion and binary Maxwell–Stefan diffusion in simple fluids with the Green–Kubo method. Int. J. Thermophys. 2004;25(1):175-86. doi: 10.1023/B:IJOT.0000022333.07168.c4.

Accepted manuscript

ACCEPTED MANUSCRIPT

[71] Van de Ven-Lucassen IMJJ, Vlugt TJH, Van der Zenden AJJ, Kerkhof PJAM. Using molecular dynamics to obtain Maxwell-Stefan diffusion coefficients in liquid systems. Mol. Phys. 1998;94(3):495-3. doi: 10.1080/002689798168006.

[72] Rothman LS, Gordon IE, Babikov Y, Barbe A, Benner D.C, Bernath PF *et al.* The HITRAN2012 molecular spectroscopic database. J. Quant. Spectrosc. Radiat. Transfer, 2013;130:4-50. doi: 10.1016/j.jqsrt.2013.07.002.

[73] Jacquinet-Husson N, Armante R, Scott NA, Chédin A, Crépeau L, Boutammine C *et al.* The 2015 edition of the GEISA spectroscopic database. J. Mol. Spectrosc. 2016; 327:31-72. doi: 10.1016/j.jms.2016.06.007.

[74] Kochanov VP. Manifestations of small-angle molecular scattering in spectral line profiles, J. Exp. Theor. Phys. 2014, ; 118(3): 335–50. doi: 10.1134/S1063776114020125.

[75] Kochanov VP. On parameterization of spectral line profiles including the speed-dependence in the case of gas mixtures. J Quant Spectrosc Radiat Transfer 2017; 189: 18–23. doi: 10.1016/j.jqsrt.2016.11.007.

[76] Tennyson J, Bernath PF, Campargue A, Császár AG, Daumont L, Gamache RR *et al.* Recommended isolated-line profile for representing high-resolution spectroscopic transitions (IUPAC Technical Report). Pure Appl. Chem. 2014; 86(12): 1931–43. doi: 10.1515/pac-2014-0208.

[77] Pine AS. N_2 and Ar broadening and line mixing in the P and R branches of theν_3 band of CH4. J Quant Spectrosc Radiat Transfer 1997; 57: 157–76. doi: 10.1016/S0022-4073(96)00130-6.

[78] Kochanov VP. Collision line narrowing and mixing of multiplet spectra. J Quant Spectrosc Radiat Transfer 2000; 66: 313–25. doi: 10.1016/S0022-4073(99)00116-8.

[79] Ciurylo R, Pine AS. Speed-dependent line mixing profiles. J Quant Spectrosc Radiat Transfer 2000; 67: 375–93. doi: .1016/S0022-4073(00)00030-3.

[80] Kochanov VP. Line profiles for the description of line mixing, narrowing, and dependence of relaxation constants on speed. J Quant Spectrosc Radiat Transfer 2011; 112: 1931–41. doi: 10.1016/j.jqsrt.2011.04.009.

[81] Kochanov VP. Speed-dependent spectral line profile including line narrowing and mixing. J Quant Spectrosc Radiat Transfer 2016; 177: 261–8. doi: 10.1016/j.jqsrt.2016.02.014.

Accepted manuscript

ACCEPTED MANUSCRIPT

[82] Cherkasov M.R. Theory of relaxation parameters of the spectrum shape in the impact approximation–I: General consideration. J Quant Spectrosc Radiat Transfer. 2014; 141. P.73-88. doi: 10.1016/j.jqsrt.2013.11.013.

List of Figures

Fig. 1. Multispectrum fits of 10 spectra of CO using the (A) Voigt, (B) Speed-Dependent Voigt, (C) Rautian, (D) Speed-Dependent Rautian profiles, all with weak line mixing, covering the region 4149.5 and 4170.5 cm^{-1} belonging to the P(20) to R(24) transition in the 2←0 band of CO.

Fig 2 Ratios of line positions (panel (A)) and line intensities (panel (B)) between our measured results and the corresponding values in the HITRAN [72] and GEISA [73] databases. Panels (C) and (D) present the measured uncertainties obtained for line positions ($\times 10^5$ cm^{-1}) and intensities ($\times 10^{25}$ cm^{-1}/(molecule·cm^{-2})), respectively.

Fig. 3. (A) Measured Lorentz self-broadened half-width coefficients of CO using the Voigt and speed-dependent Voigt (SD-Voigt) models and comparison with published results. The line shape model used is mentioned in the figure legend. (B) Sample of broadening coefficients obtained using the speed-dependent Voigt, Voigt, Rautian and speed-dependent Rautian line shape models. (C) Measured Lorentz self-broadened half-width coefficients of CO in the present study using Voigt, speed-dependent Voigt (SD-Voigt), Rautian and speed-dependent Rautian models.

Fig. 4. (A) Measured room temperature pressure-induced shift coefficients of pure CO from present study using the Voigt and speed-dependent Voigt (SD-Voigt) models and their comparisons with the literature values. (B) Room temperature self-induced pressure-shift coefficients retrieved with four different line shape models.

Fig. 5. Measured Lorentz half-width coefficient of H_2-broadened CO from the present study using the Voigt and speed-dependent Voigt models and comparisons with published results obtained using the Voigt model.

Accepted manuscript

ACCEPTED MANUSCRIPT

Fig. 6. Measured pressure-induced shift coefficients of H_2-broadened CO from present study using Voigt and speed-dependent Voigt models and their comparisons with published measurements obtained using the Voigt model.

Fig. 7. (A) Measured collisional line mixing parameter of pure CO using the Voigt and speed-dependent Voigt models compared with other published and calculated results obtained using the exponential power gap (EPG) law. (B) Measured collisional line mixing of CO-H_2 obtained using the Voigt and speed-dependent Voigt models.

Fig. 8. Speed dependence parameters for pure CO (a), and CO and H_2 mixtures (b) obtained using the speed-dependent Voigt profile.

Fig. 9. Test of convergence of thermally averaged theoretical line broadening coefficients for pure CO (panel (A)) and CO broadened by H_2 (panel (B)) with b_{max} (in Å) increasing. *J*-dependences of CO half-widths calculated using a different parameter b_{max} in the calculation. Interaction PES parameters for pure CO are ε =110 K, σ =3.59 Å [59], ρ =0.089 [60, 61]. Interaction parameters for CO broadened by H_2 are ε =48.8787 K, σ =3.3872 Å [55], ρ = 0.16667 [59].

Fig. 10. Test of the MThV approximation. Parameters of interaction PESs are the same as in Fig. 9.

Fig. 11. Comparison of theoretical with experimental results for the pure CO system. Theoretical broadening at half width half maximum coefficients was calculated using three different sets of potential energy parameters (curves 1-3). The parameters of PESs are as follows: (1) ε =110 K, σ =3.59 Å [59], ρ =0.089 [60, 61]; (2) ε =91.7 K, σ =3.690 Å [63], ρ =0.089 [61]; (3) ε =91.7 K, σ =3.690 Å [63], ρ =0.089 [60, 61]. R_{max} = 20 Å, b_{max} = 19 Å.

Fig. 12. Comparison of theoretical and experimental results for CO and H_2 mixtures. The theoretical H_2-broadening coefficients were calculated using two different sets of parameters for PESs (curves 1 and 2). The parameters of the interaction PES are as follows: (1) ε =48.8787 K, σ =3.3872 Å [53], ρ = 0.16667 [57]; (2) ε =91.7 K, σ =3.690 Å ([61] + Berthelot rules), ρ =0.089 [59]. R_{max} = 15 Å, b_{max} = 13 Å.

Accepted manuscript

ACCEPTED MANUSCRIPT

Fig. 13. Contributions of different parts of the interaction PES into CO pressure broadening coefficients for pure CO. The parameters of interaction PES correspond to Fig. 9.

Fig. 14. Contributions of different parts of interaction PES into CO pressure broadening coefficients for CO broadened by H_2. The parameters of interaction PES correspond to Fig. 9.

Table 1. Summary of experimental conditions of the measured spectra of pure CO and CO-H_2 mixtures used in this study.

Gas Sample	Temperature (K)	Total Pressure (Torr)	Volume Gas Mixture Ratio	Path Length (m)
Pure CO	298.05	97.26	1.0	0.0205
Pure CO	298.05	148.30	1.0	0.0205
Pure CO	298.05	329.50	1.0	0.0205
Pure CO	298.30	3.15	1.0	0.1
Pure CO	297.90	4.47	1.0	0.1
Pure CO	298.20	9.40	1.0	0.1
Pure CO	298.15	123.85	1.0	0.1
Pure CO	279.90	279.90	1.0	0.1
Pure CO	298.20	507.00	1.0	0.1
Pure CO	298.15	1.36	1.0	1.5
CO-H_2	298.20	155.15	0.1696	0.1
CO-H_2	298.05	315.65	0.1899	0.1
CO-H_2	297.85	474.65	0.2297	0.1
CO-H_2	275.95	94.33	0.0487	1.5
CO-H_2	275.65	174.12	0.0509	1.5
CO-H_2	275.75	332.34	0.0496	1.5
CO-H_2	296.20	574.70	0.0120	1.5
CO-H_2	296.35	643.11	0.0474	1.5

Accepted manuscript

ACCEPTED MANUSCRIPT

Table 2. Molecular parameters for CO and H_2 used in the theoretical calculations of CO line broadening coefficients.

Molecule	*r* (Å)	*B* (cm^{-1})	μ(D)	*Q* (D·Å)
$^{12}C^{16}O$	1.1309	1.9225	0.11	-2.0
H_2	0.7508	59.3345	0	0.6522

Table 3. CO-CO, H_2-H_2 and CO-H_2 Lennard-Jones interaction parameters, ε, σ, used in present calculations.

Type of Interaction	ε (K)	σ (Å)	Reference
CO-CO	110	3.59	[58]
	91.7	3.69	[62]
H_2-H_2	59.7	2.827	[62]
CO-H_2	48.8787	3.3872	[54]
	73.9898	3.2585	[62][a]

[a] Calculated from data of Ref. [62] using Lorentz-Berthelot combination rules.

Table 4. Calculated diffusion constants (cm^2/s) and friction parameter ($cm^{-1}atm^{-1}$) for pure CO and H_2 as well as for CO-H_2 mixtures with different molar fractions calculated at T=298 K and pressure of 1 atm.

Diffusion Constant for Pure CO	Diffusion Constant for Pure H_2	Volume Mixing Ratio of CO-H_2 Spectra	Diffusion Constant for gas mixture (D_{12})	Friction Parameter (β_{diff})×10^4
0.194	1.420	1 (pure CO)	0.19	242.299
		0.0120	1.41	33.424
		0.0474	1.36	34.479
		0.0487	1.36	34.530
		0.0496	1.36	34.555
		0.0509	1.36	34.581
		0.1696	1.21	38.747
		0.1899	1.19	39.563

Accepted manuscript

ACCEPTED MANUSCRIPT

	0.2297	1.14	41.266

Table 5. Optimized adjustable parameters for semi-empirical calculations using the Exponential Power Gap (EPG) method.

Constants*	CO-CO	$CO-H_2$	$CO-H_2$
	P and R	P	R
a ***($cm^{-1}atm^{-1}$)***	0.04555	0.0152	0.0181
b	0.41980	0.1280	0.1910
c	1.10630	1.2000	1.1000

*See text for details.

Table 6. Line positions, intensities and Einstein A coefficients obtained using the Speed-Dependent Voigt line shape model.

m	Line Positions (cm^{-1})	Line Intensity $\times 10^{22}$ (cm^{-1}/(molecule·cm^{-2})) at 296K	Einstein A coefficient (s^{-1})
-24	4148.797708(99)	0.559(5)	0.4246
-23	4154.212260(93)	0.840(5)	0.4291
-22	4159.560420(64)	1.231(5)	0.4371
-21	4164.841602(45)	1.770(5)	0.4434
-20	4170.055891(33)	2.504(6)	0.4464
-19	4175.203163(24)	3.487(7)	0.4495
-18	4180.283295(18)	4.747(7)	0.4518
-17	4185.296052(15)	6.272(7)	0.4588
-16	4190.241224(12)	8.123(8)	0.4647
-15	4195.118736(10)	10.310(8)	0.4697
-14	4199.928509(8)	12.694(9)	0.4800
-13	4204.670277(7)	15.588(10)	0.4790
-12	4209.343958(7)	18.369(10)	0.4858
-11	4213.949410(6)	21.171(11)	0.4921
-10	4218.486447(6)	23.804(11)	0.4961

Accepted manuscript

ACCEPTED MANUSCRIPT

-9	4222.954945(6)	25.852(12)	0.5063
-8	4227.354766(5)	27.329(12)	0.5148
-7	4231.685733(5)	27.873(12)	0.5248
-6	4235.947753(5)	27.350(12)	0.5362
-5	4240.140651(6)	25.635(12)	0.5506
-4	4244.264227(6)	22.662(12)	0.5699
-3	4248.318396(7)	18.433(11)	0.6038
-2	4252.303025(8)	13.111(10)	0.6718
-1	4256.217943(14)	6.848(9)	1.0184
1	4263.837930(14)	7.038(9)	0.3458
2	4267.542864(8)	13.901(10)	0.4193
3	4271.177403(6)	20.192(11)	0.4528
4	4274.741533(6)	25.585(12)	0.4734
5	4278.235058(5)	29.853(13)	0.4866
6	4281.657825(5)	32.875(13)	0.4978
7	4285.009711(5)	34.537(14)	0.5064
8	4288.290573(5)	34.895(14)	0.5137
9	4291.500221(5)	34.018(13)	0.5222
10	4294.638584(5)	32.210(13)	0.5274
11	4297.705411(5)	29.600(13)	0.5336
12	4300.700661(5)	26.496(12)	0.5393
13	4303.624136(6)	23.135(11)	0.5435
14	4306.475699(6)	19.687(11)	0.5496
15	4309.255182(7)	16.334(10)	0.5558
16	4311.962464(8)	13.275(9)	0.5581
17	4314.597391(9)	10.552(9)	0.5632
18	4317.159814(11)	8.208(8)	0.5667
19	4319.649574(14)	6.244(8)	0.5711
20	4322.066549(18)	4.616(7)	0.5797
21	4324.410613(24)	3.374(7)	0.5824
22	4326.681506(33)	2.401(6)	0.5869
23	4328.879349(46)	1.691(6)	0.5874

Accepted manuscript

Table 7. Line broadening coefficients ($cm^{-1}atm^{-1}$) for pure CO (Fig. 3, panel (C)) and CO-H_2 (Fig.5, panel (B)) for transitions in the first overtone band obtained using the Voigt, Speed-Dependent Voigt, Rautian and Speed-Dependent Rautian line shape models. Calculated values obtained using the EPG method are also included.

m	CO-CO					CO-H_2				
	Voigt	Rautian	SD-	SD-	EPG	Voigt	Rautian	SD-	SD-	EPG

ACCEPTED MANUSCRIPT

			Voigt	Rautian				Voigt	Rautian	
-24	0.04935 (65)	0.04994(73)	0.05008(74)	0.05043(74)	0.04537	0.0588(3 7)	0.0673(2 4)	0.05789(193)	0.05771(195)	0.05972
-23	0.05128 (47)	0.05150(52)	0.05154(52)	0.05189(52)	0.05053	0.0624(2 5)	0.0708(1 6)	0.06254(133)	0.06231(135)	0.06296
-22	0.05155 (33)	0.05196(37)	0.05193(37)	0.05232(37)	0.05309	0.0679(1 8)	0.0744(1 1)	0.06823(101)	0.06799(102)	0.06499
-21	0.05228 (25)	0.05277(27)	0.05284(27)	0.05319(27)	0.05464	0.0671(1 3)	0.0742(8)	0.06790(69)	0.06769(70)	0.06634
-20	0.05406 (19)	0.05424(21)	0.05424(21)	0.05461(21)	0.05572	0.0653(9)	0.0720(6)	0.06585(49)	0.06564(50)	0.06726
-19	0.05532 (15)	0.05530(16)	0.05542(32)	0.05498(33)	0.05656	0.0645(7)	0.0718(4)	0.06441(36)	0.06419(37)	0.06791
-18	0.05654 (13)	0.05644(13)	0.05753(28)	0.05716(32)	0.05729	0.0674(5)	0.0729(3)	0.06790(30)	0.06779(30)	0.06835
-17	0.05718 (11)	0.05743(11)	0.05718(19)	0.05650(19)	0.05797	0.0658(4)	0.0722(3)	0.06604(22)	0.06583(23)	0.06862
-16	0.0581(10)	0.05834(9)	0.05821(16)	0.05763(16)	0.05865	0.0662(3)	0.0719(2)	0.06651(18)	0.06631(19)	0.06876
-15	0.05925 (9)	0.05937(8)	0.05917(13)	0.05864(14)	0.05934	0.0674(3)	0.0718(2)	0.06747(15)	0.06731(16)	0.06878
-14	0.06004 (8)	0.06009(7)	0.06023(12)	0.05975(13)	0.06008	0.0690(2)	0.0727(2)	0.06888(13)	0.06872(14)	0.06870
-13	0.06157 (8)	0.06183(6)	0.06246(12)	0.06201(13)	0.06088	0.0685(2)	0.0716(1)	0.06865(12)	0.06852(12)	0.06853
-12	0.06242 (8)	0.06242(6)	0.06293(10)	0.06246(11)	0.06177	0.0667(2)	0.0698(1)	0.06726(11)	0.06713(11)	0.06831
-11	0.06348 (7)	0.06321(5)	0.06387(10)	0.06347(10)	0.06276	0.0690(2)	0.0712(1)	0.06899(10)	0.06887(10)	0.06804
-10	0.06432 (7)	0.06417(5)	0.06511(9)	0.06478(10)	0.06389	0.0695(2)	0.0710(1)	0.06960(9)	0.06951(10)	0.06778
-9	0.06525 (7)	0.06505(5)	0.06565(9)	0.06516(9)	0.06519	0.0694(2)	0.0708(1)	0.06952(9)	0.06943(9)	0.06755
-8	0.06617 (7)	0.06603(5)	0.06665(8)	0.06624(9)	0.06670	0.0695(2)	0.0709(1)	0.06966(9)	0.06956(9)	0.06742
-7	0.06751 (7)	0.06719(5)	0.06807(9)	0.06771(9)	0.06847	0.0692(2)	0.0708(1)	0.06934(9)	0.06925(9)	0.06744
-6	0.06995 (8)	0.06894(5)	0.06963(9)	0.06926(10)	0.07057	0.0697(2)	0.0712(1)	0.06987(9)	0.06977(9)	0.06770
-5	0.07153 (8)	0.07125(5)	0.07226(10)	0.07196(11)	0.07306	0.0697(2)	0.0717(1)	0.06985(9)	0.06974(10)	0.06831
-4	0.07416 (9)	0.07401(6)	0.07492(11)	0.07465(13)	0.07603	0.0701(2)	0.0725(1)	0.07018(10)	0.07007(10)	0.06940
-3	0.07736 (10)	0.07755(7)	0.07866(14)	0.07842(16)	0.07946	0.0702(2)	0.0737(1)	0.07034(12)	0.07021(12)	0.07113
-2	0.08100 (12)	0.08136(10)	0.08294(20)	0.08278(23)	0.08296	0.0701(3)	0.0749(2)	0.07017(15)	0.07001(15)	0.07363
-1	0.08674 (19)	0.08696(	0.08776(36)	0.08756(40)	0.08710	0.0742(5)	0.0808(3)	0.07460(28)	0.07441(28)	0.07636

Accepted manuscript

ACCEPTED MANUSCRIPT

		17)								
1	0.0864(19)	0.08659(17)	0.08796(37)	0.08772(41)	0.08743	0.0734(4)	0.0802(3)	0.07372(27)	0.07352(27)	0.07941
2	0.08171(12)	0.08174(9)	0.08287(19)	0.08265(21)	0.08367	0.0704(3)	0.0749(2)	0.07050(15)	0.07034(15)	0.07646
3	0.07754(10)	0.07749(7)	0.07852(13)	0.07822(15)	0.07859	0.0706(2)	0.0736(1)	0.07063(12)	0.07050(12)	0.07335
4	0.07444(9)	0.07531(6)	0.07516(11)	0.07486(12)	0.07463	0.0702(2)	0.0723(1)	0.07029(10)	0.07018(10)	0.07107
5	0.07147(8)	0.07241(5)	0.07225(9)	0.07194(10)	0.07160	0.0702(2)	0.0715(1)	0.07034(9)	0.07025(9)	0.06949
6	0.06908(7)	0.06873(4)	0.06965(8)	0.06929(9)	0.06925	0.0697(1)	0.0708(1)	0.06989(9)	0.06980(9)	0.06845
7	0.06718(7)	0.06706(4)	0.06772(8)	0.06732(8)	0.06739	0.0698(1)	0.0706(1)	0.06994(8)	0.06987(9)	0.06781
8	0.06577(7)	0.06560(4)	0.06636(7)	0.06593(8)	0.06589	0.0693(1)	0.0699(1)	0.06949(8)	0.06941(8)	0.06749
9	0.06473(7)	0.06453(4)	0.06515(7)	0.06469(8)	0.06467	0.0692(1)	0.0698(1)	0.06939(8)	0.06931(9)	0.06739
10	0.06382(7)	0.06367(4)	0.06426(7)	0.06380(8)	0.06363	0.0691(1)	0.0701(1)	0.06927(9)	0.06919(9)	0.06746
11	0.06283(7)	0.06280(4)	0.06328(8)	0.06279(8)	0.06274	0.0689(2)	0.0700(1)	0.06910(9)	0.06900(9)	0.06764
12	0.06185(7)	0.06189(5)	0.06229(8)	0.06178(8)	0.06194	0.0690(2)	0.0702(1)	0.06899(10)	0.06890(10)	0.06791
13	0.06095(8)	0.06102(5)	0.06144(9)	0.06088(9)	0.06121	0.0693(2)	0.0711(1)	0.06942(11)	0.06932(11)	0.06822
14	0.06007(8)	0.06019(5)	0.06051(10)	0.05995(10)	0.06052	0.0687(2)	0.0710(1)	0.06883(12)	0.06870(12)	0.06855
15	0.05882(9)	0.05904(6)	0.05924(11)	0.05861(11)	0.05984	0.0684(2)	0.0713(1)	0.06861(13)	0.06848(13)	0.06888
16	0.05767(9)	0.05802(7)	0.05804(12)	0.05745(12)	0.05916	0.0677(2)	0.0718(2)	0.06778(15)	0.06763(15)	0.06918
17	0.05681(10)	0.05697(8)	0.05704(14)	0.05644(15)	0.05844	0.0670(3)	0.0716(2)	0.06732(18)	0.06714(18)	0.06943
18	0.05568(12)	0.05625(9)	0.05645(18)	0.05577(18)	0.05767	0.0670(3)	0.0722(2)	0.06750(22)	0.06733(22)	0.06961
19	0.05481(14)	0.05501(11)	0.05525(22)	0.05458(22)	0.05680	0.0674(4)	0.0729(3)	0.06792(28)	0.06774(28)	0.06969
20	0.05326(17)	0.05352(14)	0.05352(14)	0.05398(14)	0.05576	0.0665(5)	0.0734(3)	0.06684(35)	0.06663(35)	0.06961
21	0.05217(21)	0.0525(18)	0.05246(18)	0.05293(18)	0.05443	0.0650(7)	0.0717(4)	0.06534(46)	0.06515(46)	0.06930
22	0.05092(26)	0.05191(24)	0.05143(24)	0.05191(24)	0.05256	0.0645(9)	0.0724(6)	0.06477(62)	0.06459(62)	0.06861
23	0.05073(36)	0.05112(32)	0.05064(32)	0.05113(32)	0.04966	0.0649(13)	0.0722(8)	0.06555(90)	0.06532(91)	0.06729

Accepted manuscript

ACCEPTED MANUSCRIPT

24	0.04432	0.0666(20)	0.0731(13)	0.06855(148)	0.06813(144)	0.06483	

Table 8. Pressure-induced line shift coefficients (cm^{-1} atm^{-1}) for CO-CO and CO-H_2 for transitions in the first overtone band obtained using the Voigt, Speed-Dependent Voigt, Rautian and Speed-Dependent Rautian line shape models.

m	CO-CO				CO-H_2			
	Voigt	Rautian	SD-Voigt	SD-Rautian	Voigt	Rautian	SD-Voigt	SD-Rautian
-24	-0.00652(70)	-0.00669(65)	-0.00668(64)	-0.00670(65)	0.0006(29)	0.0004(33)	0.0024(17)	0.0025(17)
-23	-0.00677(52)	-0.00668(46)	-0.00668(45)	-0.00667(46)	-0.0040(20)	-0.0043(22)	-0.0051(12)	-0.0051(12)
-22	-0.00502(36)	-0.00640(32)	-0.00640(32)	-0.00640(32)	-0.0115(15)	-0.0121(16)	-0.0110(9)	-0.0110(9)
-21	-0.00619(27)	-0.00610(24)	-0.00609(24)	-0.00609(24)	-0.008(10)	-0.0082(11)	-0.0076(6)	-0.0076(6)
-20	-0.00541(21)	-0.00561(18)	-0.00561(18)	-0.00561(18)	-0.0075(7)	-0.0077(8)	-0.0077(4)	-0.0077(4)
-19	-0.00531(16)	-0.00546(14)	-0.00547(14)	-0.00547(14)	-0.0070(6)	-0.0073(6)	-0.0075(3)	-0.0074(3)
-18	-0.00511(16)	-0.00536(14)	-0.00550(11)	-0.00552(11)	-0.0062(5)	-0.0064(6)	-0.0068(3)	-0.0068(3)
-17	-0.00508(13)	-0.00560(11)	-0.00546(9)	-0.00548(9)	-0.0065(4)	-0.0066(4)	-0.0064(2)	-0.0064(2)
-16	-0.00513(12)	-0.00549(9)	-0.00553(8)	-0.00554(8)	-0.0053(3)	-0.0054(3)	-0.0053(2)	-0.0053(2)
-15	-0.00525(10)	-0.00549(8)	-0.00553(7)	-0.00554(7)	-0.0062(3)	-0.0063(3)	-0.0062(2)	-0.0062(2)
-14	-0.00508(10)	-0.00574(7)	-0.00573(6)	-0.00573(6)	-0.0055(2)	-0.0056(2)	-0.0056(1)	-0.0056(1)
-13	-0.00499(9)	-0.00534(5)	-0.00534(5)	-0.00534(5)	-0.0051(2)	-0.0052(2)	-0.0052(1)	-0.0052(1)

Accepted manuscript

ACCEPTED MANUSCRIPT

-12	-0.00471(9)	-0.00512(5)	-0.00512(5)	-0.00512(5)	-0.0052(2)	-0.0052(2)	-0.0051(1)	-0.0051(1)
-11	-0.00482(8)	-0.00526(5)	-0.00525(5)	-0.00526(5)	-0.0045(2)	-0.0046(2)	-0.0045(1)	-0.0045(1)
-10	-0.00471(8)	-0.00501(5)	-0.00507(4)	-0.00508(4)	-0.0046(2)	-0.0047(2)	-0.0046(1)	-0.0047(1)
-9	-0.00465(8)	-0.00501(5)	-0.00503(4)	-0.00502(4)	-0.0047(2)	-0.0047(2)	-0.0046(1)	-0.0046(1)
-8	-0.00443(8)	-0.00490(5)	-0.00488(4)	-0.00489(4)	-0.0053(2)	-0.0053(2)	-0.0054(1)	-0.0054(1)
-7	-0.00422(8)	-0.00464(5)	-0.00466(4)	-0.00467(4)	-0.0047(2)	-0.0048(2)	-0.0049(1)	-0.0049(1)
-6	-0.00413(7)	-0.00456(5)	-0.00459(4)	-0.00460(4)	-0.0046(2)	-0.0046(2)	-0.0047(1)	-0.0047(1)
-5	-0.00428(9)	-0.00455(5)	-0.00461(5)	-0.00461(5)	-0.0051(2)	-0.0052(2)	-0.0053(1)	-0.0053(1)
-4	-0.00349(9)	-0.00400(6)	-0.00398(5)	-0.00399(5)	-0.0047(2)	-0.0047(2)	-0.0048(1)	-0.0048(1)
-3	-0.00299(10)	-0.00354(6)	-0.00354(6)	-0.00354(6)	-0.0047(2)	-0.0048(2)	-0.0049(1)	-0.0049(1)
-2	-0.00293(13)	-0.00323(8)	-0.00322(8)	-0.00323(8)	-0.0051(2)	-0.0052(2)	-0.0055(2)	-0.0055(2)
-1	-0.00308(20)	-0.00328(14)	-0.00327(14)	-0.00328(14)	-0.0040(4)	-0.0041(4)	-0.0046(3)	-0.0046(3)
1	-0.00286(20)	-0.00298(14)	-0.00298(14)	-0.00297(14)	-0.0065(4)	-0.0066(4)	-0.0067(2)	-0.0067(2)
2	-0.00323(13)	-0.00362(8)	-0.00359(8)	-0.00360(8)	-0.0055(2)	-0.0057(2)	-0.0059(2)	-0.0059(2)
3	-0.00327(10)	-0.00371(6)	-0.00369(6)	-0.00370(6)	-0.0044(2)	-0.0045(2)	-0.0046(1)	-0.0046(1)
4	-0.00362(9)	-0.00393(5)	-0.00394(5)	-0.00395(5)	-0.0049(2)	-0.0050(2)	-0.0052(1)	-0.0051(1)
5	-0.00367(9	-0.00411(4)	-0.00412(4	-0.00412(4	-0.0044(2)	-0.0044(2)	-0.0047(1)	-0.0047(1)

Accepted manuscript

ACCEPTED MANUSCRIPT

	)		)	)				
6	-0.00381(8)	-0.00423(4)	-0.00422(4)	-0.00422(4)	-0.0044(2)	-0.0045(2)	-0.0047(1)	-0.0048(1)
7	-0.00394(8)	-0.00433(4)	-0.00433(4)	-0.00434(4)	-0.0043(2)	-0.0043(2)	-0.0046(1)	-0.0046(1)
8	-0.00396(8)	-0.00439(4)	-0.00438(4)	-0.00438(4)	-0.0042(2)	-0.0042(2)	-0.0043(1)	-0.0043(1)
9	-0.00385(8)	-0.00429(4)	-0.00428(4)	-0.00428(4)	-0.0042(2)	-0.0042(2)	-0.0044(1)	-0.0044(1)
10	-0.00403(8)	-0.00444(4)	-0.00443(4)	-0.00444(4)	-0.0037(2)	-0.0037(2)	-0.0038(1)	-0.0038(1)
11	-0.00394(8)	-0.00434(4)	-0.00434(4)	-0.00434(4)	-0.0035(2)	-0.0036(2)	-0.0037(1)	-0.0037(1)
12	-0.00413(8)	-0.00445(4)	-0.00445(4)	-0.00445(4)	-0.0044(2)	-0.0044(2)	-0.0046(1)	-0.0046(1)
13	-0.00424(9)	-0.00461(4)	-0.00460(4)	-0.00461(4)	-0.0037(2)	-0.0038(2)	-0.0039(1)	-0.0039(1)
14	-0.00416(9)	-0.00472(5)	-0.00471(5)	-0.00472(5)	-0.0042(2)	-0.0042(2)	-0.0042(1)	-0.0042(1)
15	-0.00427(10)	-0.00463(5)	-0.00463(5)	-0.00464(5)	-0.0042(2)	-0.0042(2)	-0.0042(1)	-0.0042(1)
16	-0.00432(11)	-0.00479(6)	-0.00479(6)	-0.00480(6)	-0.0047(3)	-0.0047(3)	-0.0052(2)	-0.0051(2)
17	-0.00421(12)	-0.00469(7)	-0.00468(7)	-0.00469(7)	-0.0043(3)	-0.0045(3)	-0.0045(2)	-0.0045(2)
18	-0.00475(14)	-0.00506(8)	-0.00506(8)	-0.00506(8)	-0.0041(3)	-0.0043(3)	-0.0040(2)	-0.0040(2)
19	-0.00438(16)	-0.00491(10)	-0.00491(10)	-0.00492(10)	-0.0038(4)	-0.0040(4)	-0.0040(3)	-0.0040(3)
20	-0.00507(20)	-0.00505(12)	-0.00505(12)	-0.00505(12)	-0.0054(4)	-0.0057(5)	-0.0050(3)	-0.0050(3)
21	-0.00456(25)	-0.00488(15)	-0.00488(15)	-0.00488(15)	-0.0041(6)	-0.0044(6)	-0.0052(4)	-0.0052(4)
22	-	-	-	-	-	-	-	-

Accepted manuscript

ACCEPTED MANUSCRIPT

	0.00509(26)	0.00529(20)	0.00529(20)	0.00529(20)	0.0037(8)	0.0039(8)	0.0041(5)	0.0041(5)
23	-0.00497(36)	-0.00500(28)	-0.00500(28)	-0.00500(28)	-0.0056(11)	-0.006(11)	-0.0054(8)	-0.0054(8)
24					-0.0091(15)	-0.0095(16)	-0.0093(11)	-0.0092(11)

Table 9. Line mixing coefficients (atm^{-1}) for CO-CO and CO-H_2 for transitions in the first overtone band obtained using the Voigt, Speed-Dependent Voigt line shape models. Calculated values obtained using the EPG method are also included.

m	CO-CO			CO-H_2		
	Voigt	SD-Voigt	EPG	Voigt	SD-Voigt	EPG
-24			0.0030			0.0054
-23			0.0020			0.0049
-22			0.0018			0.0047
-21			0.0017			0.0046
-20			0.0017			0.0045
-19			0.0016	0.0042(2)	0.0040(1)	0.0044
-18	-0.0030(22)	-0.00291(10)	0.0015	0.019(37)	0.0194(19)	0.0043
-17	-0.0004(17)	-0.00159(11)	0.0015	0.0044(2)	0.0037(1)	0.0042
-16	0.0000(14)	-0.00026(8)	0.0014	0.0038(1)	0.0036(1)	0.0041
-15	0.0018(11)	0.00187(14)	0.0013	0.0042(1)	0.0040(1)	0.0039
-14	0.0023(10)	0.00167(7)	0.0012	0.0071(1)	0.0074(1)	0.0037
-13	0.0048(8)	0.00435(6)	0.0011	0.0033(1)	0.0031(0)	0.0035
-12	0.0028(7)	0.00224(7)	0.0009	0.0026(1)	0.0029(0)	0.0032
-11	0.0015(7)	0.00158(6)	0.0007	0.0031(1)	0.0029(0)	0.0028
-10	0.0001(6)	-0.00017(6)	0.0005	0.0029(1)	0.0027(0)	0.0024
-9	0.0000(6)	-0.00002(5)	0.0002	0.0017(1)	0.0018(0)	0.0019
-8	-0.0003(6)	-0.00061(6)	-0.0002	0.0011(1)	0.0015(0)	0.0013
-7	-0.0011(6)	-0.00145(6)	-0.0007	0.0001(1)	0.0006(0)	0.0006
-6	-0.0011(0)	-0.00113(6)	-0.0014	-0.0004(1)	-0.0003(0)	-0.0003
-5	0.0016(6)	0.00171(5)	-0.0024	-0.0004(1)	-0.0007(0)	-0.0013
-4	-0.0012(7)	-0.00167(6)	-0.0038	-0.0020(1)	-0.0019(0)	-0.0025
-3	-0.0047(9)	-0.00512(6)	-0.0059	-0.0029(1)	-0.0031(0)	-0.0038
-2	-0.0045(12)	-0.00469(8)	-0.0099	-0.0065(1)	-0.0061(1)	-0.0064
-1	-0.0017(22)	-0.00184(21)	-0.0194	-0.0162(2)	-0.0163(1)	-0.0145
1	0.0104(22)	0.00952(11)	0.0236	0.0101(1)	0.0100(1)	0.0093

Accepted manuscript

ACCEPTED MANUSCRIPT

2	0.0045(12)	0.00476(6)	0.0128	0.0110(1)	0.0119(1)	0.0121
3	0.0033(8)	0.00280(6)	0.0076	0.0059(1)	0.0062(1)	0.0068
4	0.0034(7)	0.00325(5)	0.0053	0.0041(1)	0.0038(0)	0.0044
5	0.0023(6)	0.00208(5)	0.0037	0.0025(1)	0.0023(0)	0.0027
6	0.0012(5)	0.00085(5)	0.0026	0.0007(1)	0.0011(0)	0.0014
7	0.0011(5)	0.00085(5)	0.0018	0.0002(1)	-0.0002(0)	0.0002
8	0.0003(5)	0.00048(5)	0.0011	-0.001(1)	-0.0011(0)	-0.0008
9	-0.0013(5)	-0.00123(5)	0.0006	-0.0019(1)	-0.0018(0)	-0.0017
10	-0.0009(6)	-0.00110(6)	0.0001	-0.0026(1)	-0.0028(0)	-0.0026
11	-0.0012(6)	-0.00089(5)	-0.0003	-0.0035(1)	-0.0032(0)	-0.0033
12	-0.0026(7)	-0.00288(6)	-0.0007	-0.0033(1)	-0.0038(0)	-0.0040
13	-0.0016(7)	-0.00127(9)	-0.0010	-0.0048(1)	-0.0041(0)	-0.0047
14	-0.0019(9)	-0.00287(7)	-0.0013	-0.0043(1)	-0.0046(1)	-0.0053
15	-0.0043(10)	-0.00423(8)	-0.0016	-0.0055(1)	-0.0052(1)	-0.0059
16	-0.0034(12)	-0.00450(7)	-0.0019	0.0005(15)	0.0004(9)	-0.0065
17	-0.0073(15)	-0.00804(11)	-0.0021	-0.0060(1)	-0.0061(1)	-0.0070
18	-0.0023(18)	-0.00256(11)	-0.0024	-0.0066(1)	-0.0067(1)	-0.0076
19	-0.0055(23)	-0.00629(15)	-0.0026	-0.0068(1)	-0.0066(1)	-0.0081
20	-0.0012(31)	-0.00054(15)	-0.0029	-0.0069(1)	-0.0074(1)	-0.0087
21	-0.0051(41)	-0.00612(19)	-0.0032	-0.0084(2)	-0.0073(1)	-0.0093
22			-0.0036			-0.0101
23			-0.0045			-0.0112
24			-0.0074			-0.0132

Table 10. Speed dependence parameter for pure CO (present study and Ref. [11]), and for CO-H_2 for transitions in the first overtone band obtained using the Speed-Dependent Voigt line shape model.

m	**CO-CO Present study**	**CO-CO Devi *et al.*, 2012**	**CO-H_2 Present study**
-24		0.083	0.00625
-23		0.071	0.00444
-22		0.066	0.00413
-21		0.070	0.00439
-20		0.064	0.00401
-19	0.086	0.070	0.00438
-18	0.140	0.070	0.00000
-17	0.044	0.071	0.00444
-16	0.056	0.068	0.00426
-15	0.046	0.074	0.00463
-14	0.077	0.070	0.00438
-13	0.111	0.073	0.00456
-12	0.103	0.074	0.00462

Accepted manuscript

ACCEPTED MANUSCRIPT

-11	0.110	0.077	0.00481
-10	0.125	0.078	0.00487
-9	0.106	0.085	0.00531
-8	0.104	0.087	0.00544
-7	0.118	0.096	0.00600
-6	0.104	0.103	0.00644
-5	0.119	0.107	0.00669
-4	0.108	0.109	0.00681
-3	0.114	0.107	0.00669
-2	0.132	0.104	0.00650
-1	0.088	0.107	0.00669
1	0.113	0.106	0.00662
2	0.110	0.105	0.00656
3	0.109	0.111	0.00694
4	0.122	0.117	0.00731
5	0.123	0.116	0.00725
6	0.118	0.112	0.00700
7	0.106	0.106	0.00073
8	0.114	0.098	0.00613
9	0.108	0.093	0.00644
10	0.107	0.088	0.00550
11	0.100	0.084	0.00525
12	0.096	0.080	0.00500
13	0.099	0.077	0.00481
14	0.092	0.076	0.00475
15	0.088	0.077	0.00481
16	0.074	0.077	0.00000
17	0.084	0.075	0.00469
18	0.097	0.076	0.00476
19	0.098	0.073	0.00457
20		0.074	0.00463
21		0.072	0.00451
22		0.069	0.00432
23		0.069	0.00432
24		0.065	0.01877

Accepted manuscript

ACCEPTED MANUSCRIPT

Table 11. Thermally averaged theoretical line broadening coefficients convergence for different b_{max} values, as shown in Fig. 9. Note that all the values are calculated in $cm^{-1}atm^{-1}$ at 296 K.

	CO-CO			CO-H_2		
J	**b_{max}=14**	**b_{max} =19**	**b_{max} =25**	**b_{max} =12**	**b_{max} =13**	**b_{max} =15**
0	0.09974	0.10075	0.10202	0.07854	0.07792	0.07857
2	0.08928	0.08974	0.08875	0.07572	0.07551	0.07578
4	0.08136	0.08108	0.08088	0.07392	0.07453	0.07422
6	0.07726	0.07667	0.07603	0.07331	0.07316	0.07311
8	0.07320	0.07265	0.07338	0.07169	0.07159	0.07224
10	0.06981	0.06899	0.06855	0.07018	0.06993	0.07008
12	0.06463	0.06466	0.06492	0.06934	0.06916	0.06944
14	0.06045	0.06091	0.06039	0.06810	0.06837	0.06853
16	0.05616	0.05661	0.05568	0.06725	0.06742	0.06708
18	0.05231	0.05255	0.05137	0.06713	0.06664	0.06635
20	0.04867	0.04847	0.04743	0.06705	0.06662	0.06664
22	0.04517	0.04522	0.04404	0.06584	0.06609	0.06643
24	0.04222	0.04227	0.04130	0.06602	0.06603	0.06640

Table 12. Theoretical line broadening coefficients in cm^{-1} atm^{-1} at 296 K obtained applying the Maxwell-Boltzmann speed averaging and Mean Thermal Velocity (MThV) approximation shown in Fig. 10.

J	CO-CO		CO-H_2	
	Maxwell-Boltzmann Average	**MThV**	**Maxwell-Boltzmann Average**	**MThV**
0	0.10075	0.10109	0.07792	0.07346
2	0.08974	0.09041	0.07551	0.07191
4	0.08108	0.08076	0.07453	0.07229
6	0.07667	0.07543	0.07316	0.07258
8	0.07265	0.07183	0.07159	0.07190
10	0.06899	0.06762	0.06993	0.07065
12	0.06466	0.06403	0.06916	0.06889
14	0.06091	0.05945	0.06837	0.06689
16	0.05661	0.05537	0.06742	0.06566
18	0.05255	0.05042	0.06664	0.06513
20	0.04847	0.04662	0.06662	0.06443
22	0.04522	0.04345	0.06609	0.06449
24	0.04227	0.04075	0.06603	0.06462

Accepted manuscript

ACCEPTED MANUSCRIPT

Table 13. Thermally averaged theoretical line broadening coefficients (cm^{-1} atm^{-1}) at 296 K shown in Figs. 10 and 11.

	CO-CO			$CO-H_2$	
J	**1**	**2**	**3**	**1**	**2**
0	0.10075	0.10012	0.10079	0.07792	0.07947
2	0.08974	0.08847	0.08901	0.07551	0.07724
4	0.08108	0.08020	0.08023	0.07453	0.07641
6	0.07667	0.07547	0.07579	0.07316	0.07563
8	0.07265	0.07154	0.07142	0.07159	0.07450
10	0.06899	0.06796	0.06800	0.06993	0.07321
12	0.06466	0.06363	0.06356	0.06916	0.07282
14	0.06091	0.05998	0.05968	0.06837	0.07180
16	0.05661	0.05523	0.05504	0.06742	0.07075
18	0.05255	0.05106	0.05086	0.06664	0.07037
20	0.04847	0.04685	0.04658	0.06662	0.06997
22	0.04522	0.04335	0.04314	0.06609	0.06986
24	0.04227	0.04029	0.04020	0.06603	0.06960

CO-CO: R_{max} = 20 Å, b_{max} = 19 Å. Parameters of interaction PES are given as follows: ***1.*** ε =110 K, σ =3.59 Å, γ =0.089; ***2.*** ε =91.7 K, σ =3.690 Å, γ =0.089; ***3.*** ε =91.7 K, σ =3.690 Å, γ =0.089.

$CO-H_2$: R_{max} = 15 Å, b_{max} = 13 Å. Parameters of interaction PES are given as follows: ***1.*** ε =48.8787 K, σ =3.3872 Å, γ = 0.16667; ***2.*** ε =91.7 K, σ =3.690 Å, γ =0.089.

Table 14. Thermally averaged line broadening coefficients (cm^{-1} atm^{-1}) at 296 K resulting from contribution of different parts of the interaction PES in the case of CO-CO and $CO-H_2$ shown in Fig. 13 and Fig. 14.

J	CO-CO				$CO-H_2$		
	TH	**TH+dd**	**TH+dd+QQ**	**TH+dd+dQ+QQ**	**TH**	**TH+QQ**	**TH+dQ+QQ**
0	0.06548	0.06559	0.09969	0.10075	0.06236	0.07845	0.07792
2	0.05720	0.05741	0.08811	0.08974	0.05954	0.07593	0.07551

Accepted manuscript

ACCEPTED MANUSCRIPT

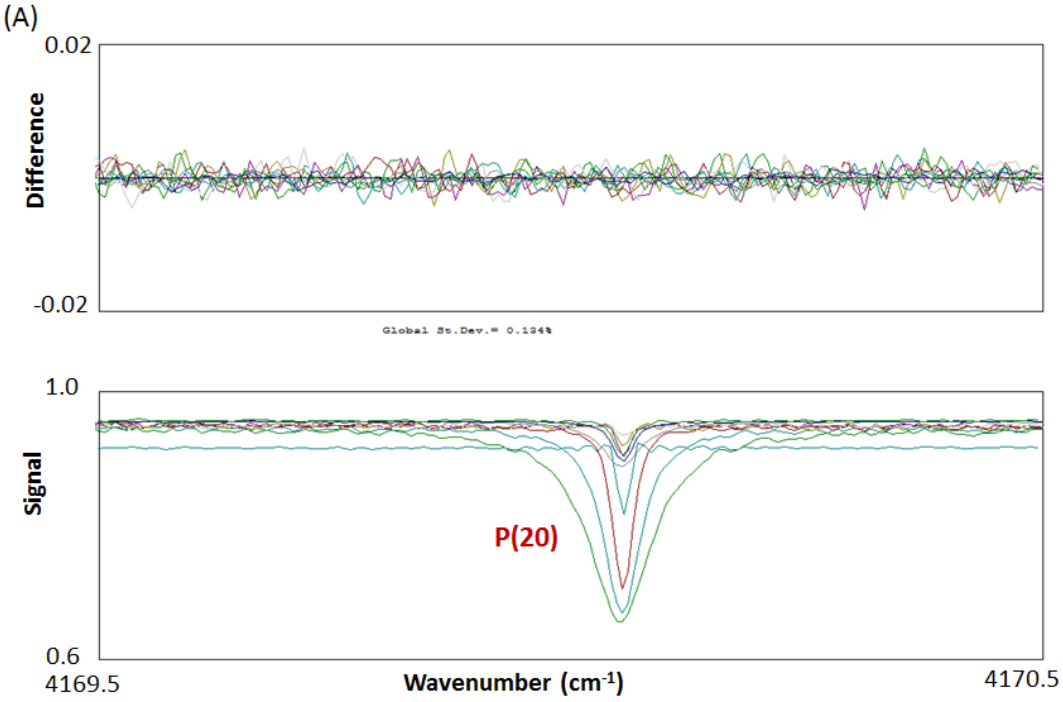
4	0.05205	0.05211	0.07924	0.08108	0.05846	0.07497	0.07453
6	0.04886	0.04873	0.07491	0.07667	0.05727	0.0735	0.07316
8	0.04745	0.04754	0.07162	0.07265	0.05724	0.07196	0.07159
10	0.04719	0.04730	0.06795	0.06899	0.05764	0.07033	0.06993
12	0.04677	0.04678	0.06407	0.06466	0.05803	0.06910	0.06916
14	0.04599	0.04602	0.06017	0.06091	0.05900	0.06837	0.06837
16	0.04534	0.04527	0.05610	0.05661	0.05926	0.06762	0.06742
18	0.04357	0.04352	0.05196	0.05255	0.05938	0.06689	0.06664
20	0.04232	0.04228	0.04787	0.04847	0.05957	0.06666	0.06662
22	0.04087	0.04088	0.04457	0.04522	0.05989	0.06622	0.06609
24	0.03925	0.03922	0.04166	0.04227	0.05985	0.06643	0.06603

Accepted manuscript

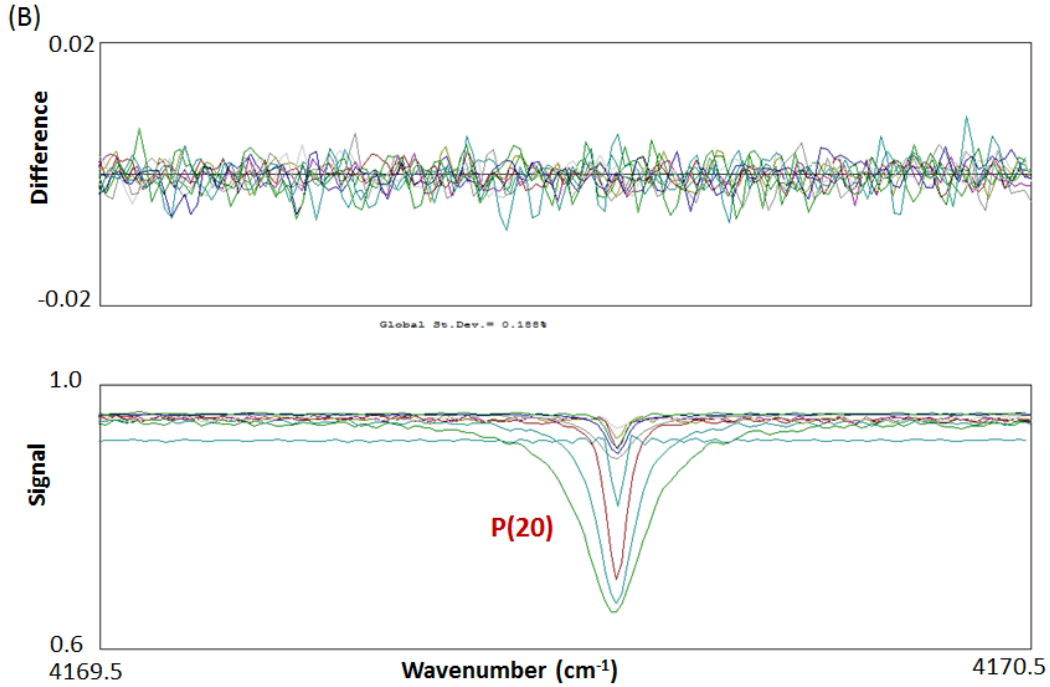
Highlights

- Self- and H_2-broadened line parameters for transitions in the 2←0 band of CO at 298 K are reported
- Line intensities, pressure shifts, line mixing and speed dependence parameters are presented.
- Calculations of self- and H_2-broadening coefficients of CO using classical impact theory are included.

Multispectrum fits of 10 spectra of CO using the Voigt model and weak line mixing

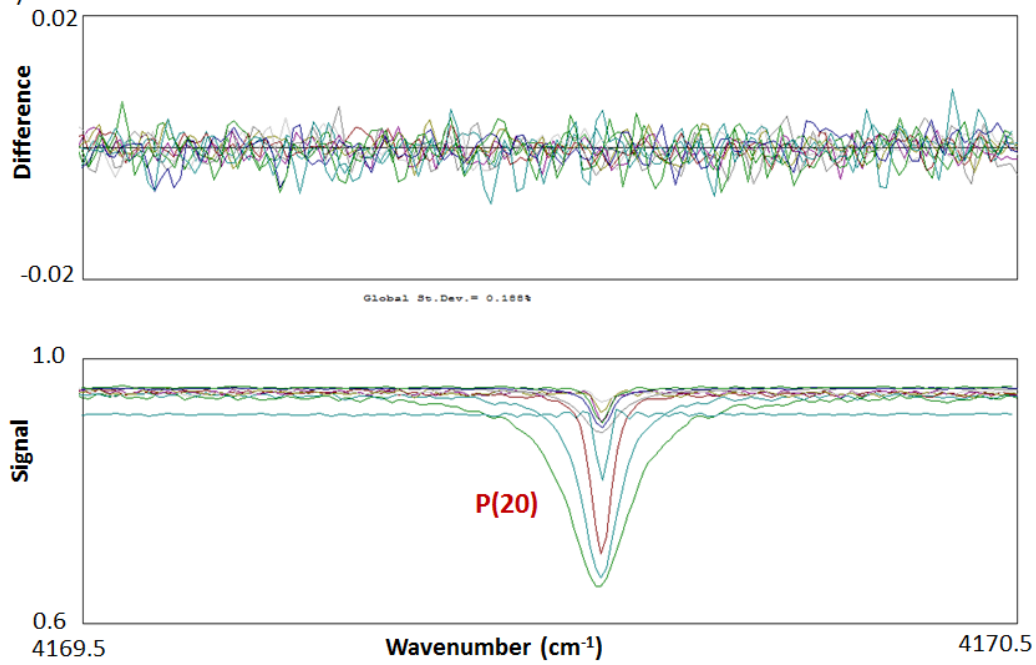


Multispectrum fits of 10 spectra of CO using the SD-Voigt model and weak line mixing



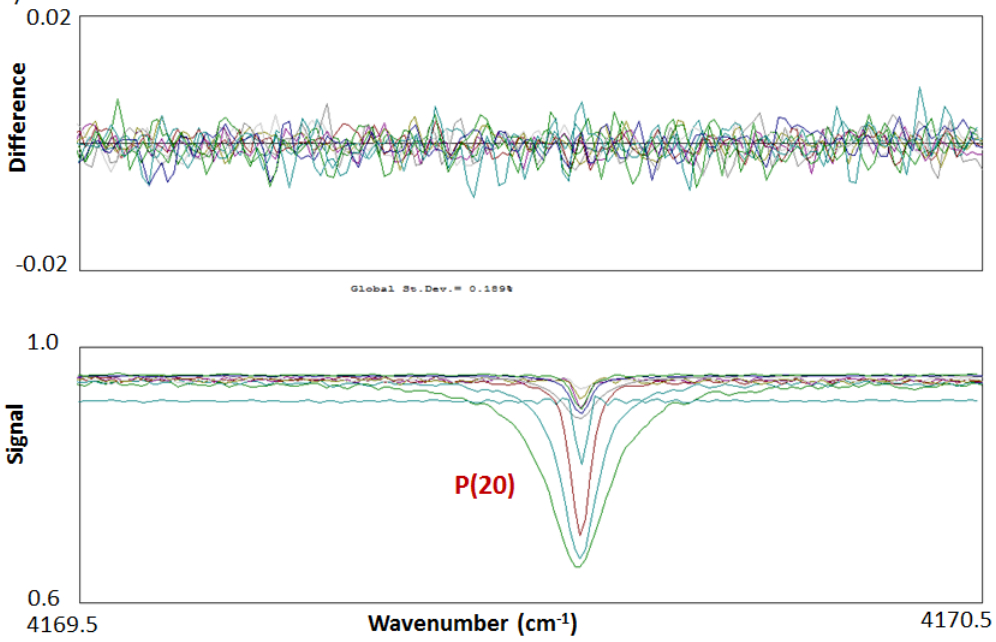
Multispectrum fits of 10 spectra of CO using the Rautian model and weak line mixing

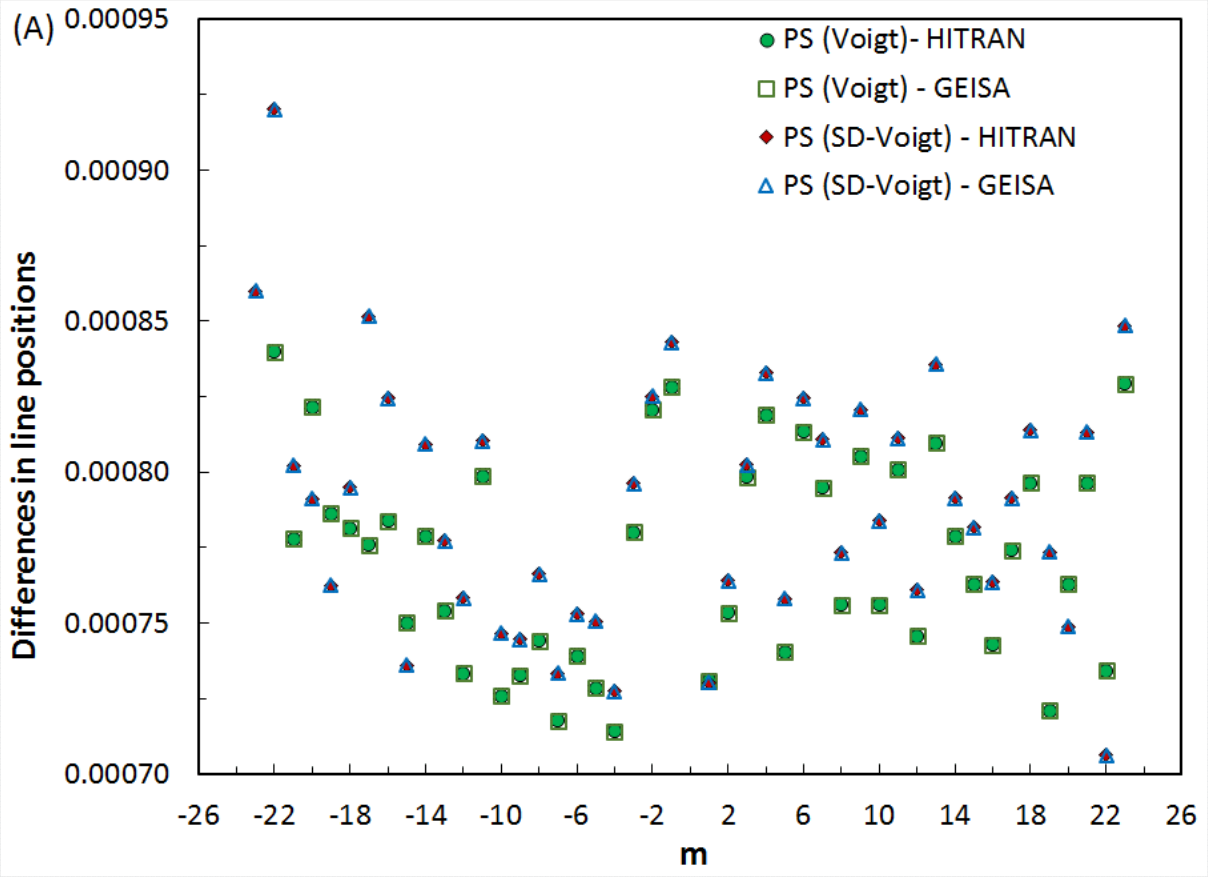
(C)



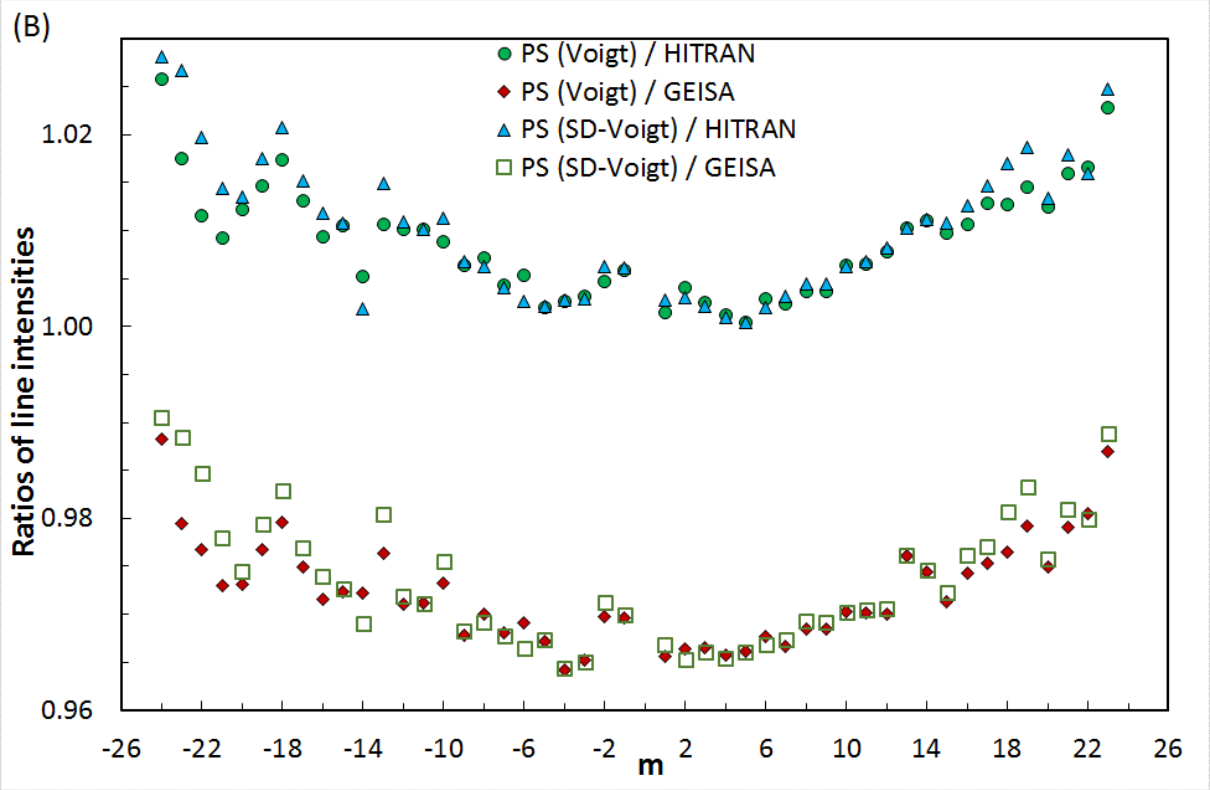
Multispectrum fits of 10 spectra of CO using the SD-Rautian model and weak line mixing

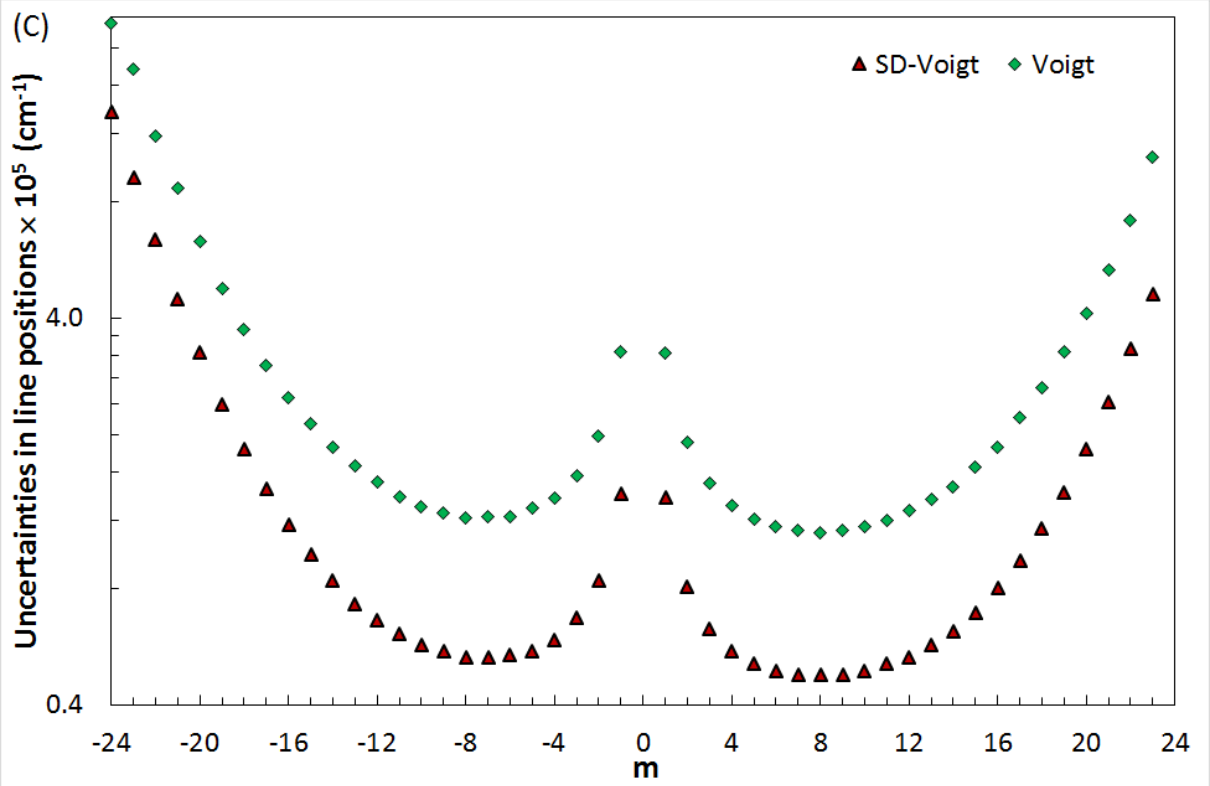
(D)

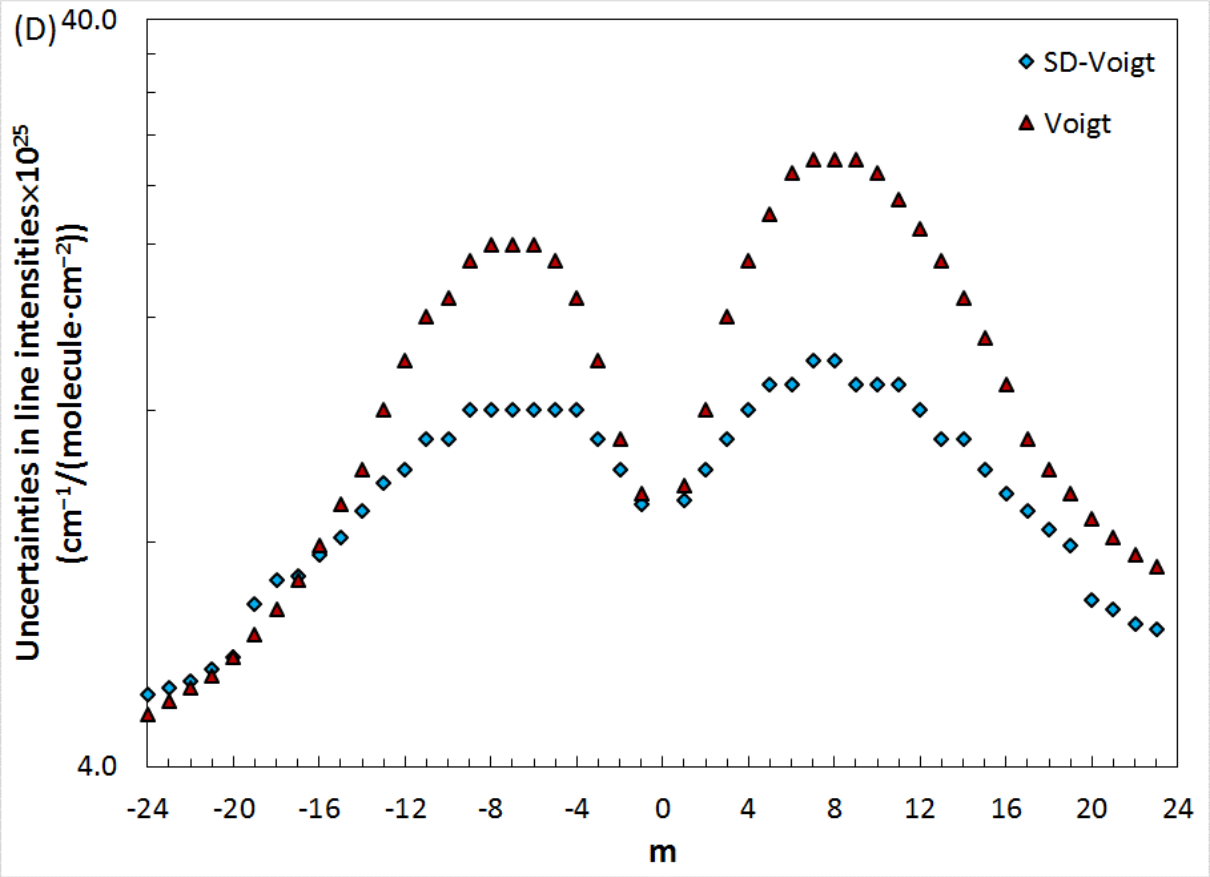



(A)
PS (Voigt)- HITRAN
PS (Voigt) - GEISA
PS (SD-Voigt) - HITRAN
PS (SD-Voigt) - GEISA
Differences in line positions
0.00095
0.00090
0.00085
0.00080
0.00075
0.00070
-26
-22
-18
-14
-10
-6
-2
2
6
10
14
18
22
26
m

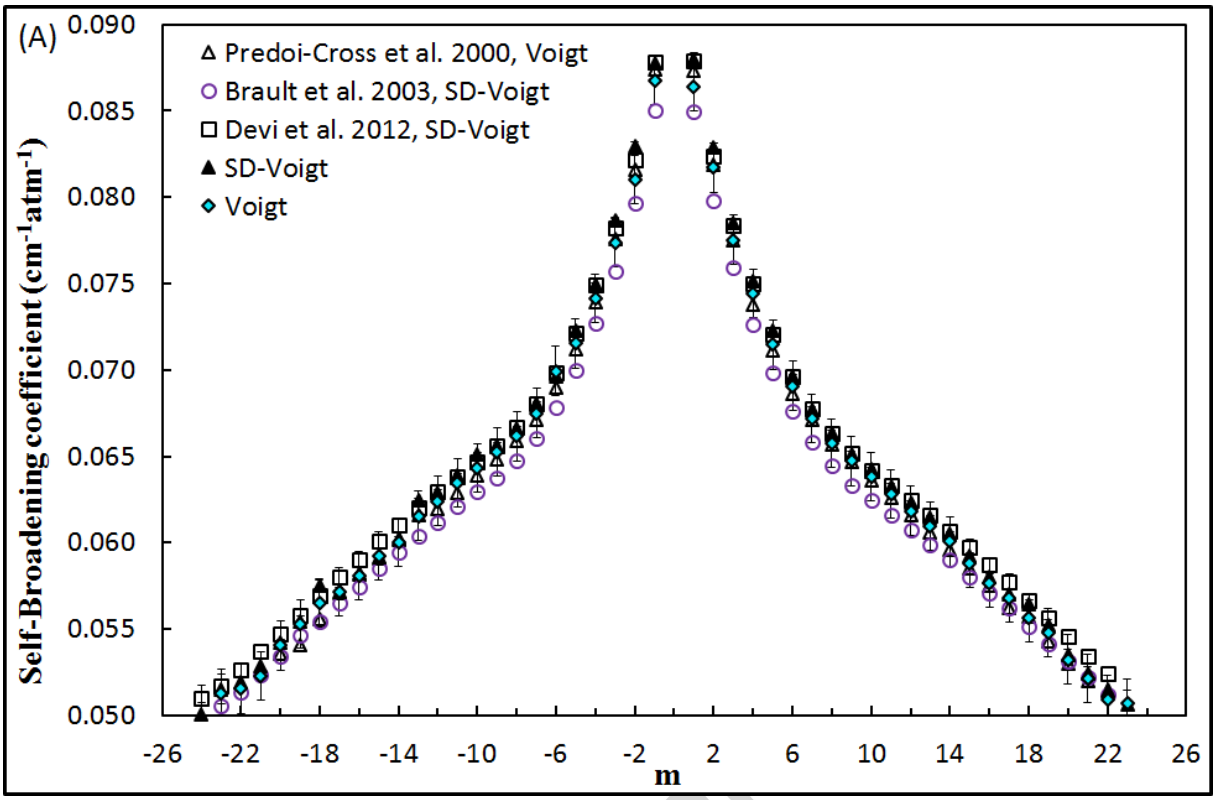
Accepted

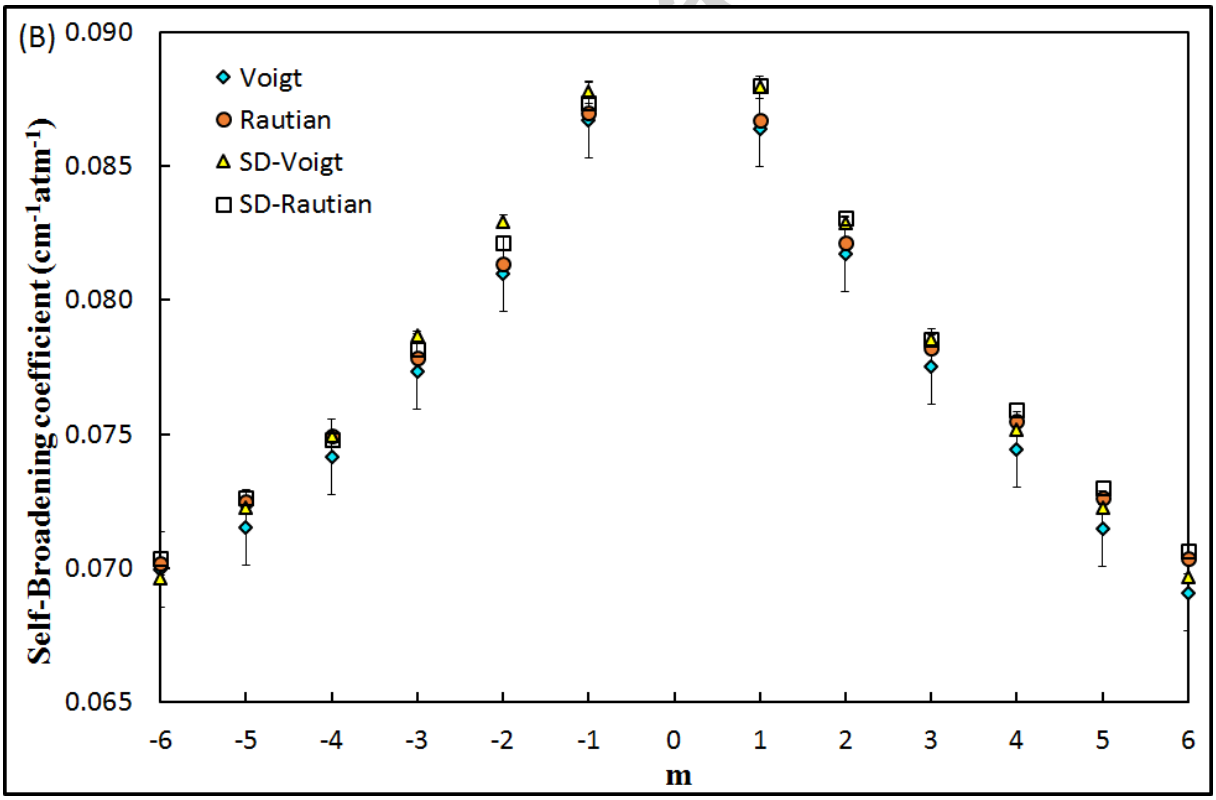

(B)
PS (Voigt) / HITRAN
PS (Voigt) / GEISA
PS (SD-Voigt) / HITRAN
PS (SD-Voigt) / GEISA
Ratios of line intensities
1.02
1.00
0.98
0.96
-26 -22 -18 -14 -10 -6 -2 2 6 10 14 18 22 26
m

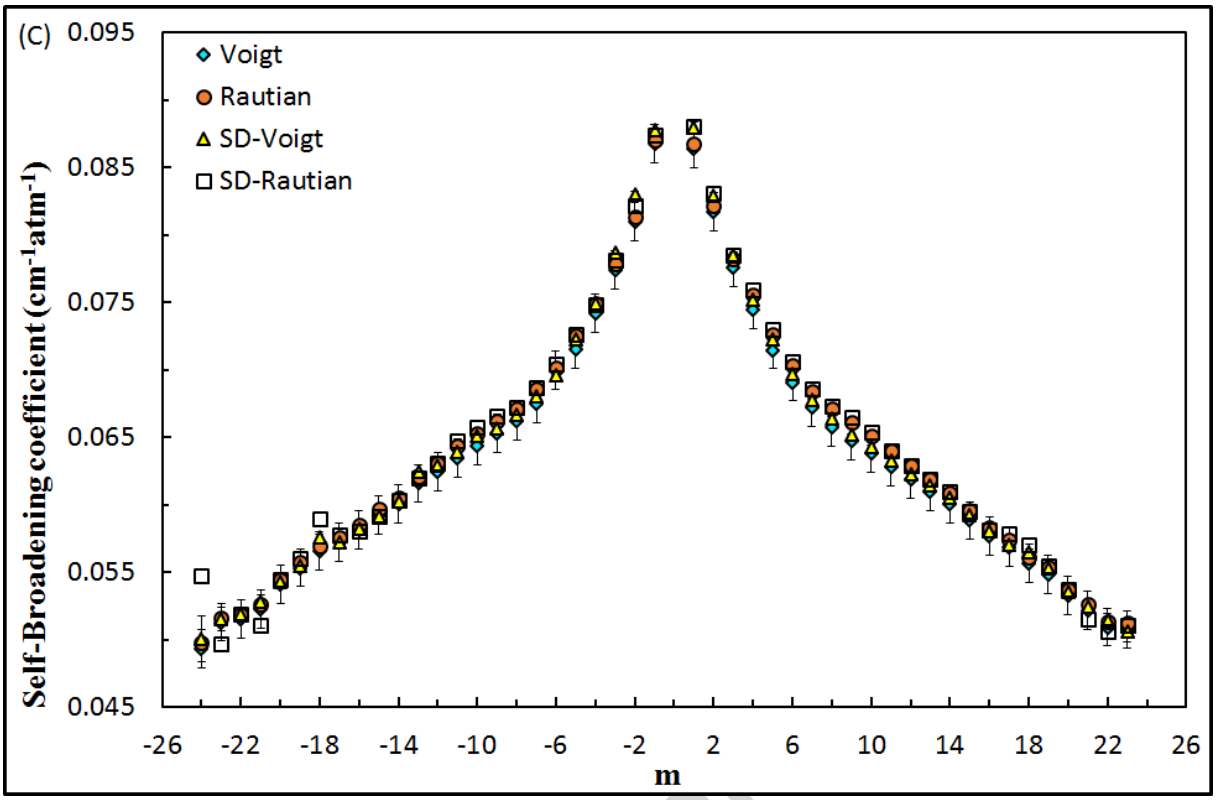

(C)
SD-Voigt
Voigt
Uncertainties in line positions × 10⁵ (cm⁻¹)
4.0
0.4
-24 -20 -16 -12 -8 -4 0 4 8 12 16 20 24
m


(D)
40.0
4.0
SD-Voigt
Voigt
Uncertainties in line intensities×10^25
(cm^-1/(molecule·cm^-2))
-24
-20
-16
-12
-8
-4
0
4
8
12
16
20
24
m

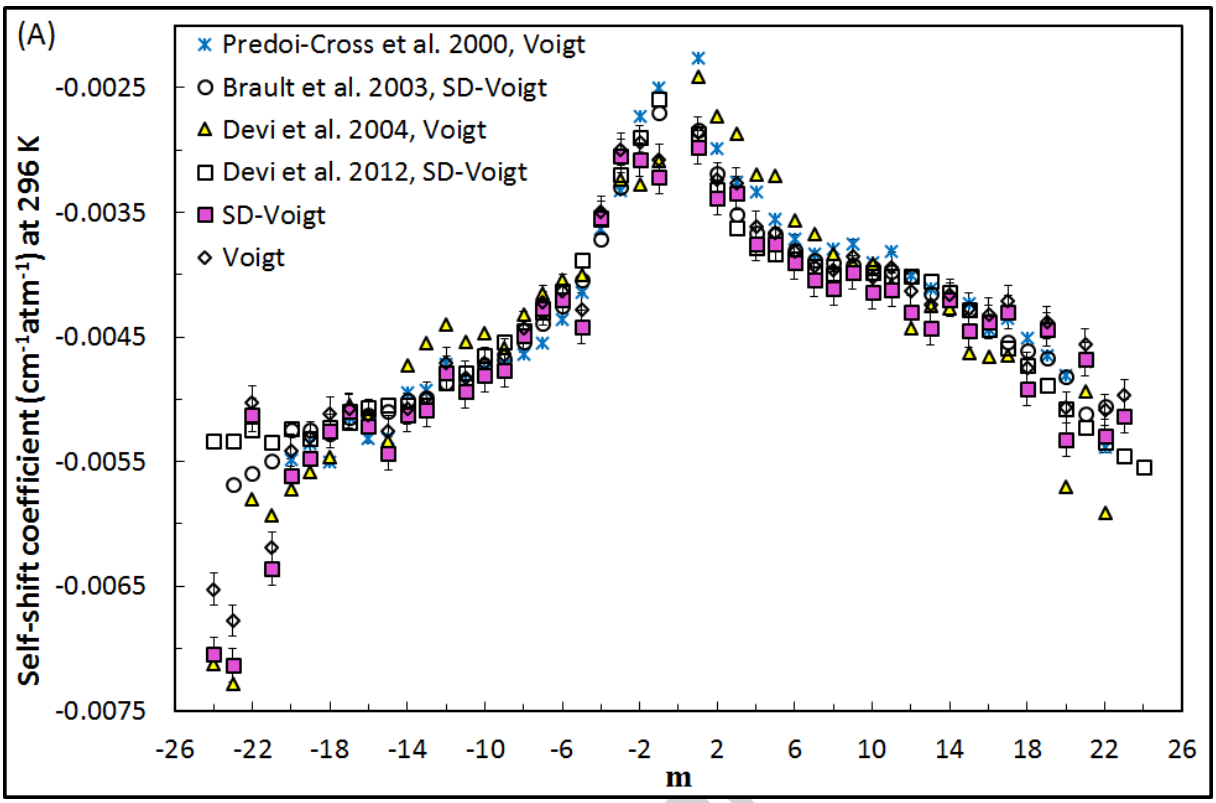
Accepted M

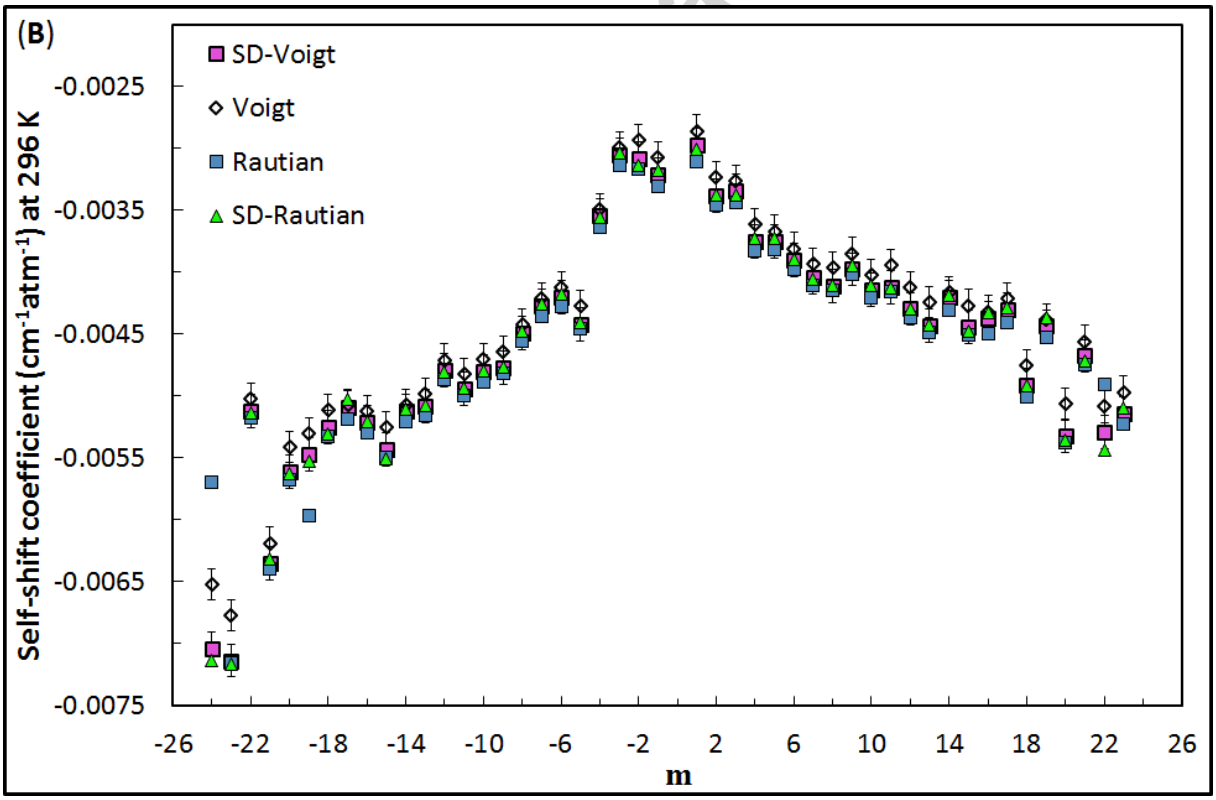

(A)
Predoi-Cross et al. 2000, Voigt
Brault et al. 2003, SD-Voigt
Devi et al. 2012, SD-Voigt
SD-Voigt
Voigt
Self-Broadening coefficient (cm-1atm-1)
0.090
0.085
0.080
0.075
0.070
0.065
0.060
0.055
0.050
-26 -22 -18 -14 -10 -6 -2 2 6 10 14 18 22 26
m

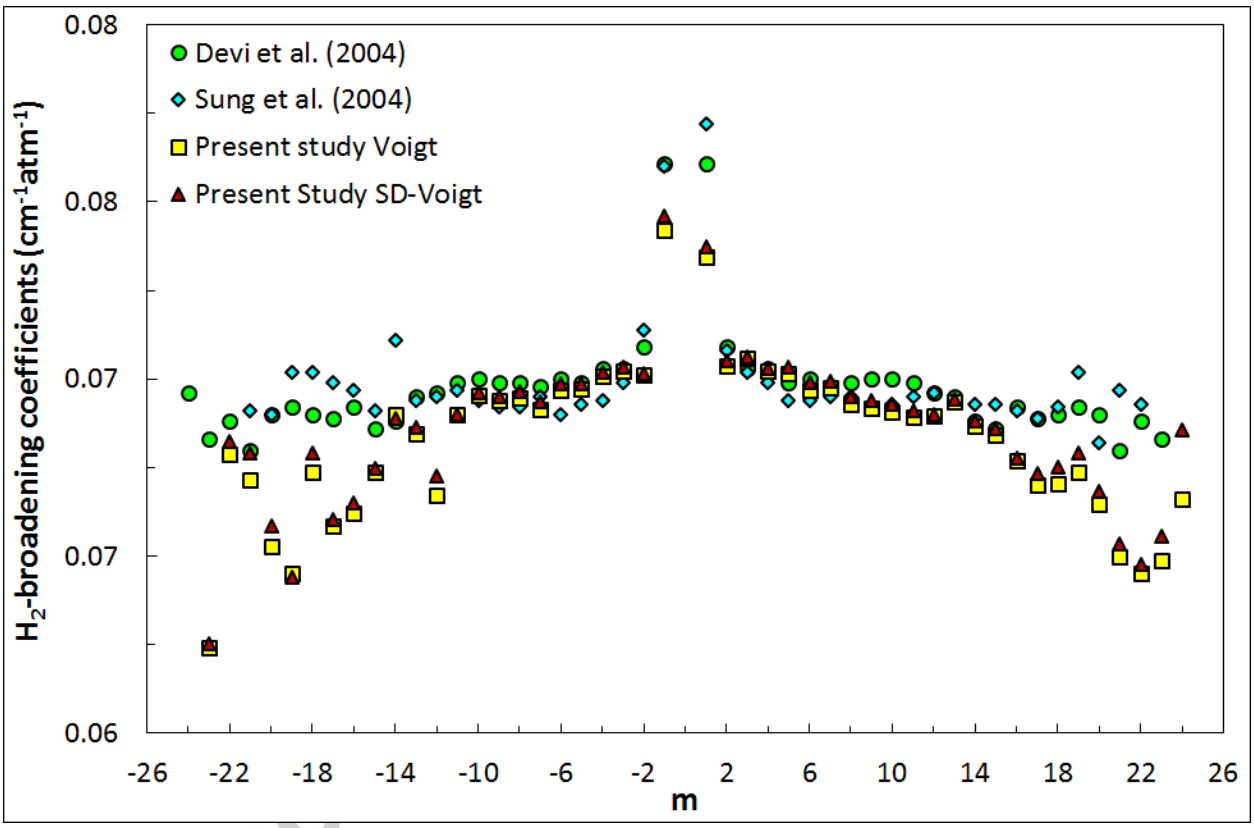

(B)
Voigt
Rautian
SD-Voigt
SD-Rautian
Self-Broadening coefficient (cm-1atm-1)
0.090
0.085
0.080
0.075
0.070
0.065
-6 -5 -4 -3 -2 -1 0 1 2 3 4 5 6
m

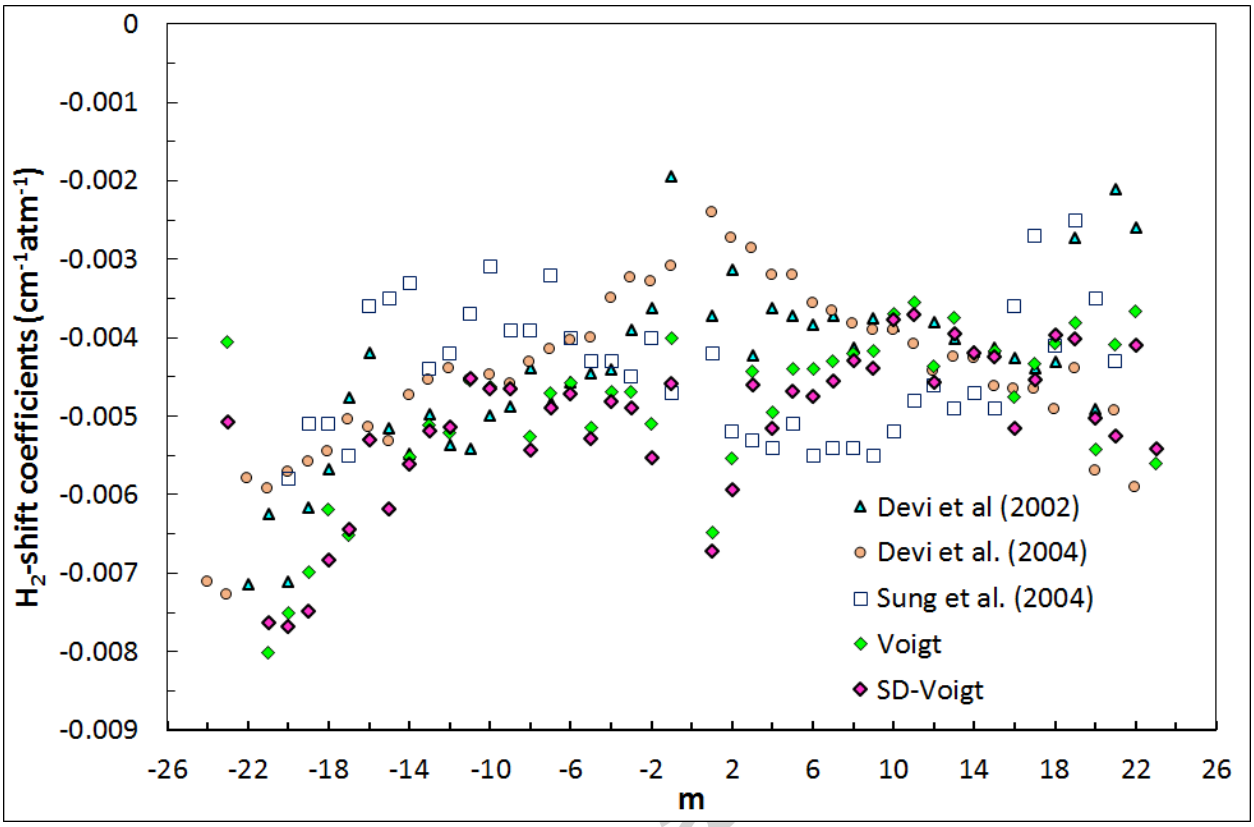


Accepted manuscript

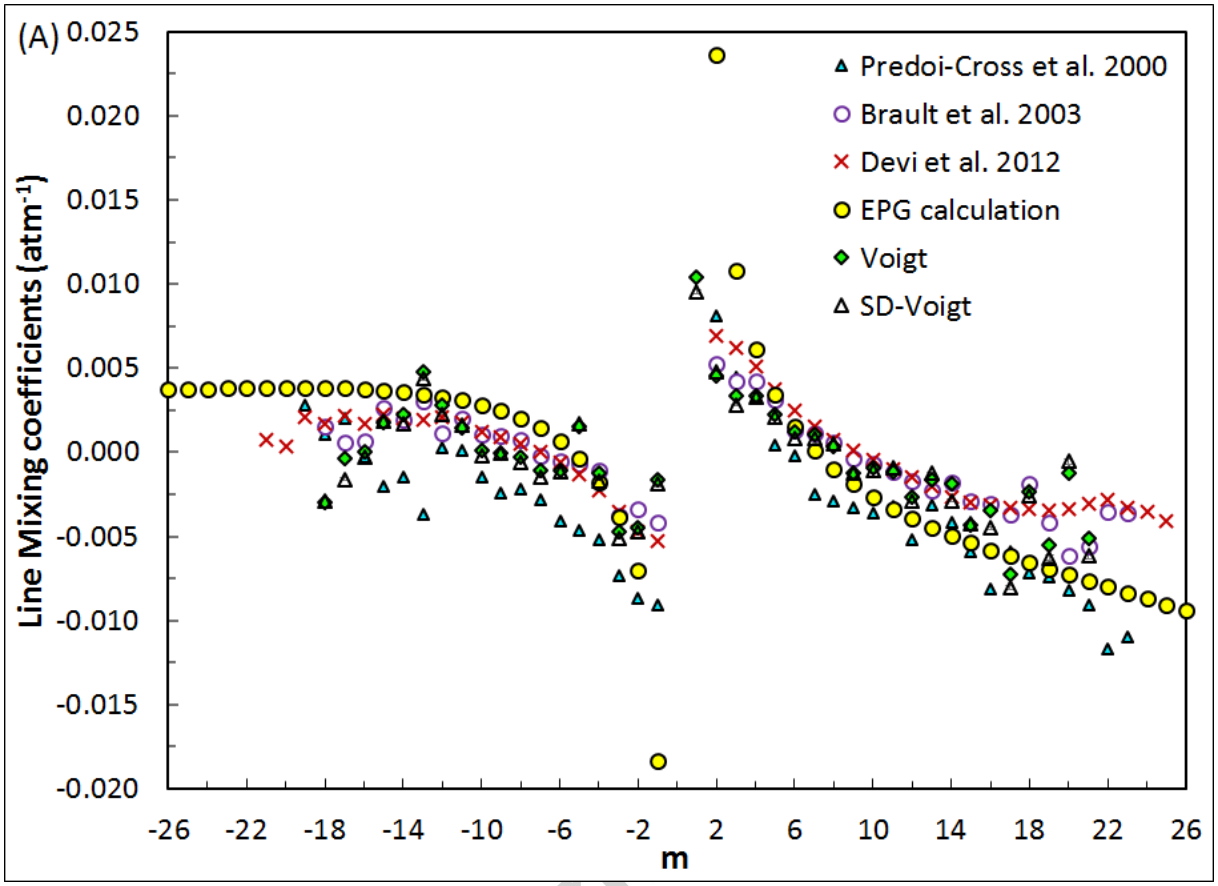

(A)
Predoi-Cross et al. 2000, Voigt
Brault et al. 2003, SD-Voigt
Devi et al. 2004, Voigt
Devi et al. 2012, SD-Voigt
SD-Voigt
Voigt
Self-shift coefficient (cm-1atm-1) at 296 K
-0.0025
-0.0035
-0.0045
-0.0055
-0.0065
-0.0075
-26 -22 -18 -14 -10 -6 -2 2 6 10 14 18 22 26
m

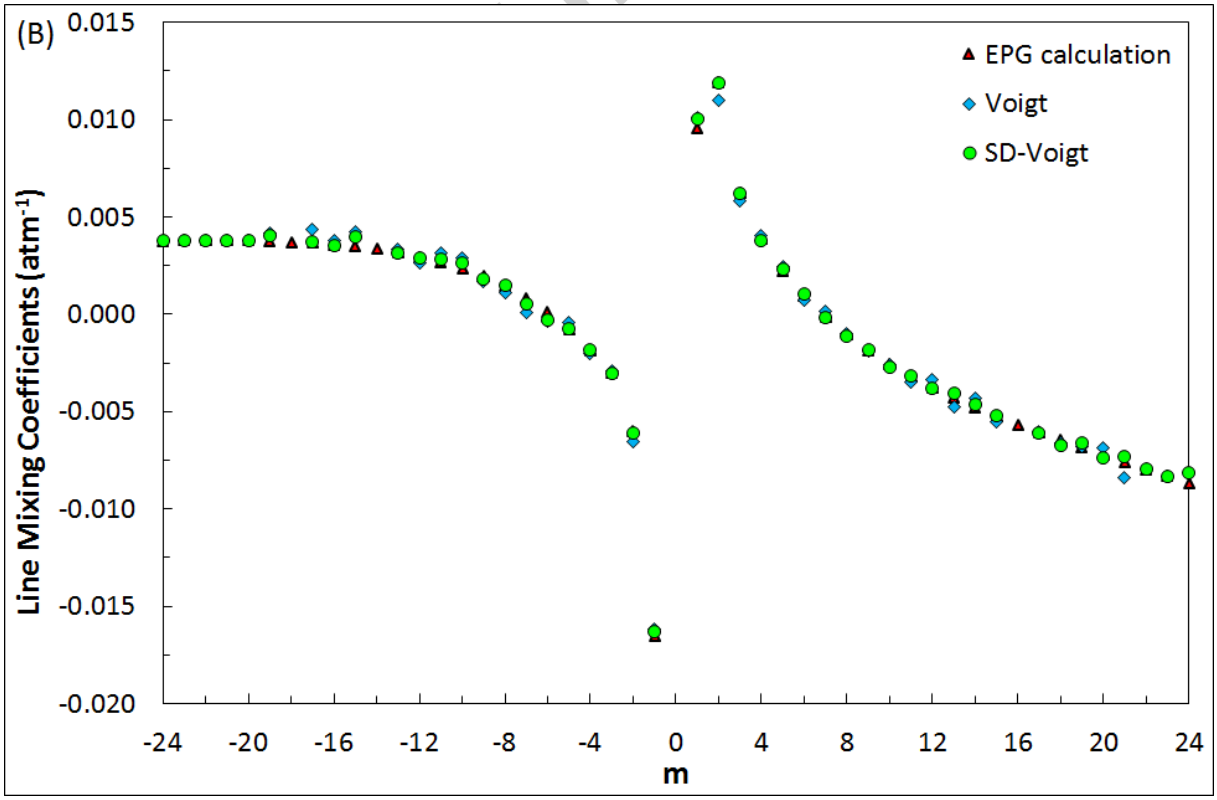

(B)
SD-Voigt
Voigt
Rautian
SD-Rautian
Self-shift coefficient (cm-1atm-1) at 296 K
-0.0025
-0.0035
-0.0045
-0.0055
-0.0065
-0.0075
-26 -22 -18 -14 -10 -6 -2 2 6 10 14 18 22 26
m

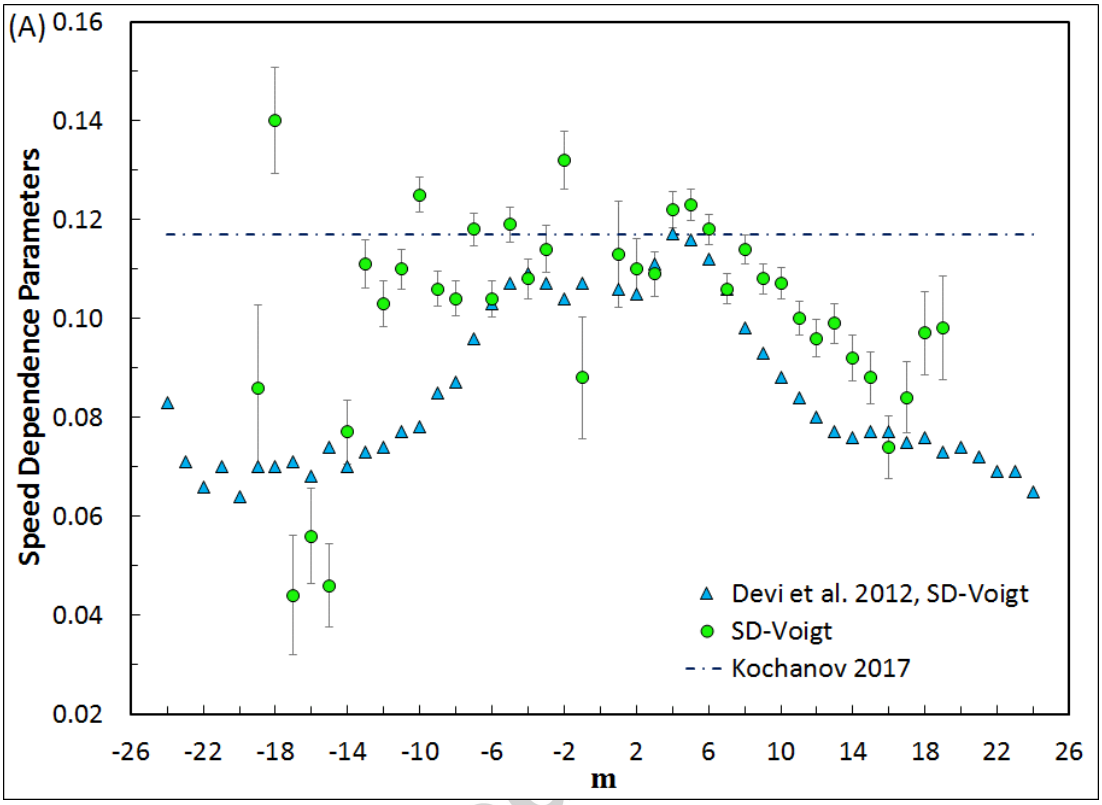

Devi et al. (2004)
Sung et al. (2004)
Present study Voigt
Present Study SD-Voigt
H2-broadening coefficients (cm-1atm-1)
0.08
0.08
0.07
0.07
0.06
-26
-22
-18
-14
-10
-6
-2
2
6
10
14
18
22
26
m


0
-0.001
-0.002
-0.003
-0.004
-0.005
-0.006
-0.007
-0.008
-0.009
H2-shift coefficients (cm-1atm-1)
-26
-22
-18
-14
-10
-6
-2
2
6
10
14
18
22
26
m
Devi et al (2002)
Devi et al. (2004)
Sung et al. (2004)
Voigt
SD-Voigt

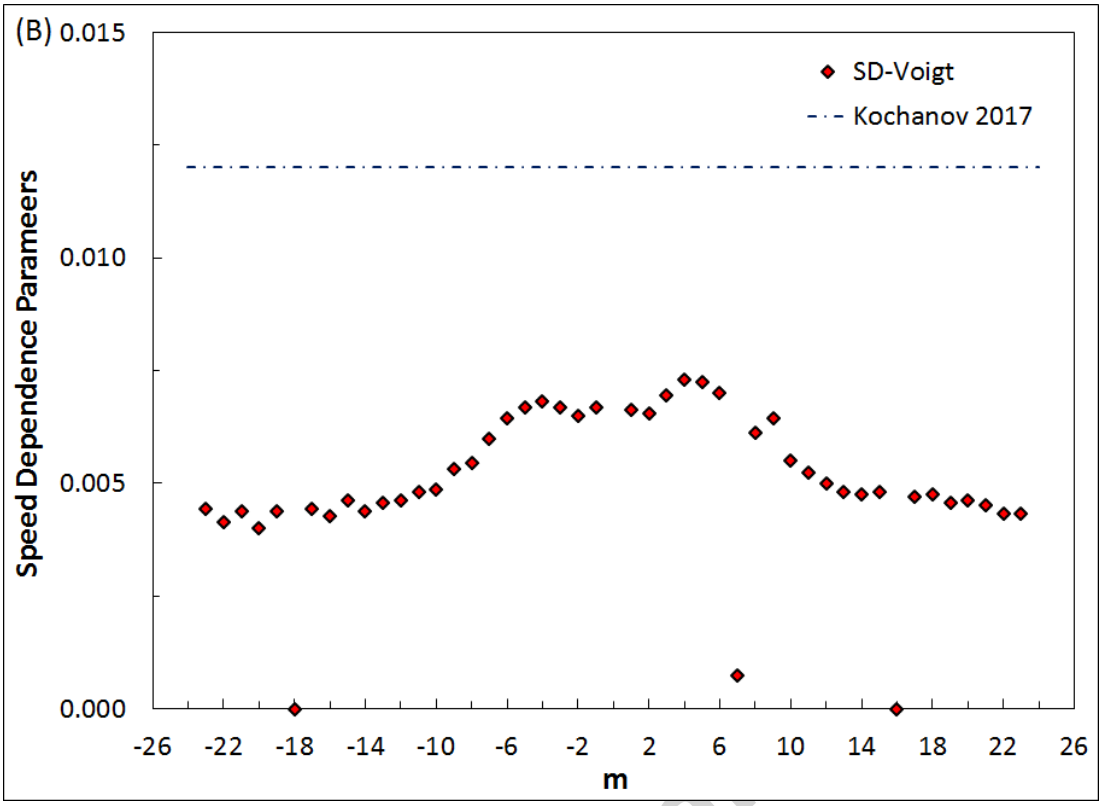
Accepted ma


(A)
Predoi-Cross et al. 2000
Brault et al. 2003
Devi et al. 2012
EPG calculation
Voigt
SD-Voigt
Line Mixing coefficients (atm-1)
m

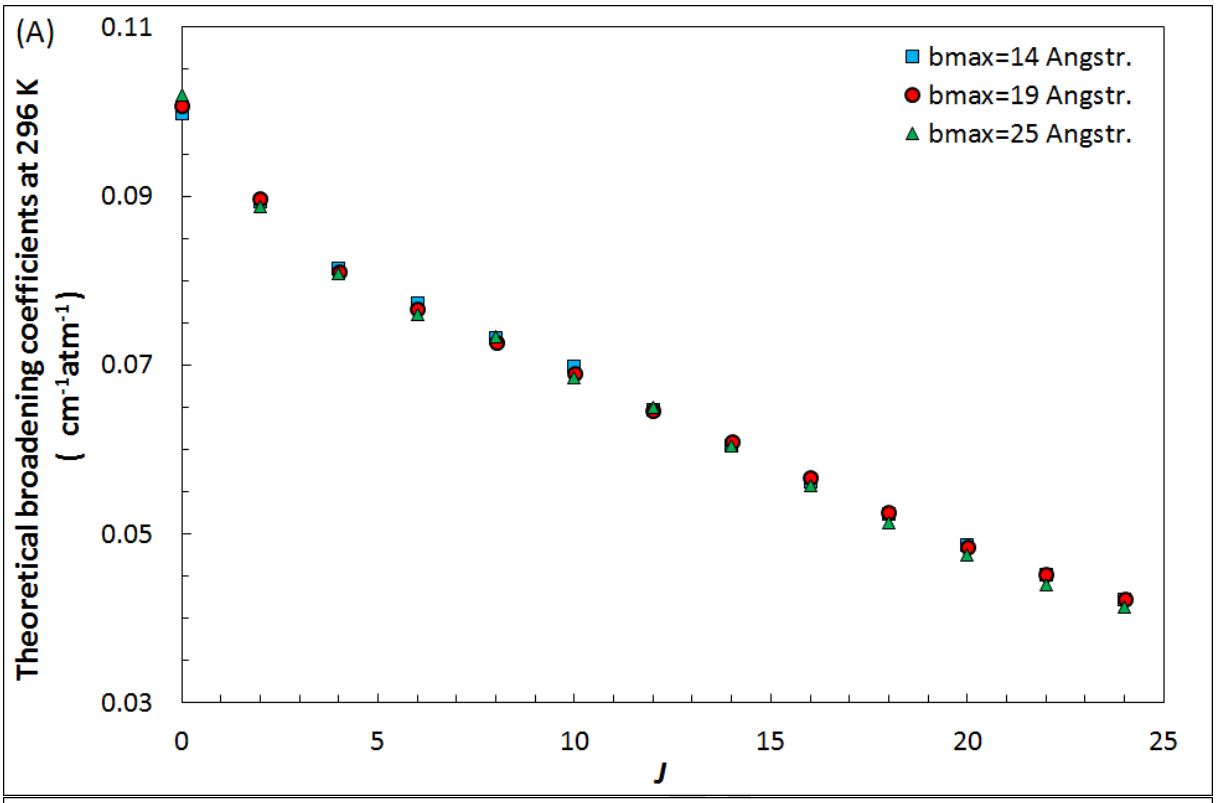

(B)
EPG calculation
Voigt
SD-Voigt
Line Mixing Coefficients (atm-1)
m

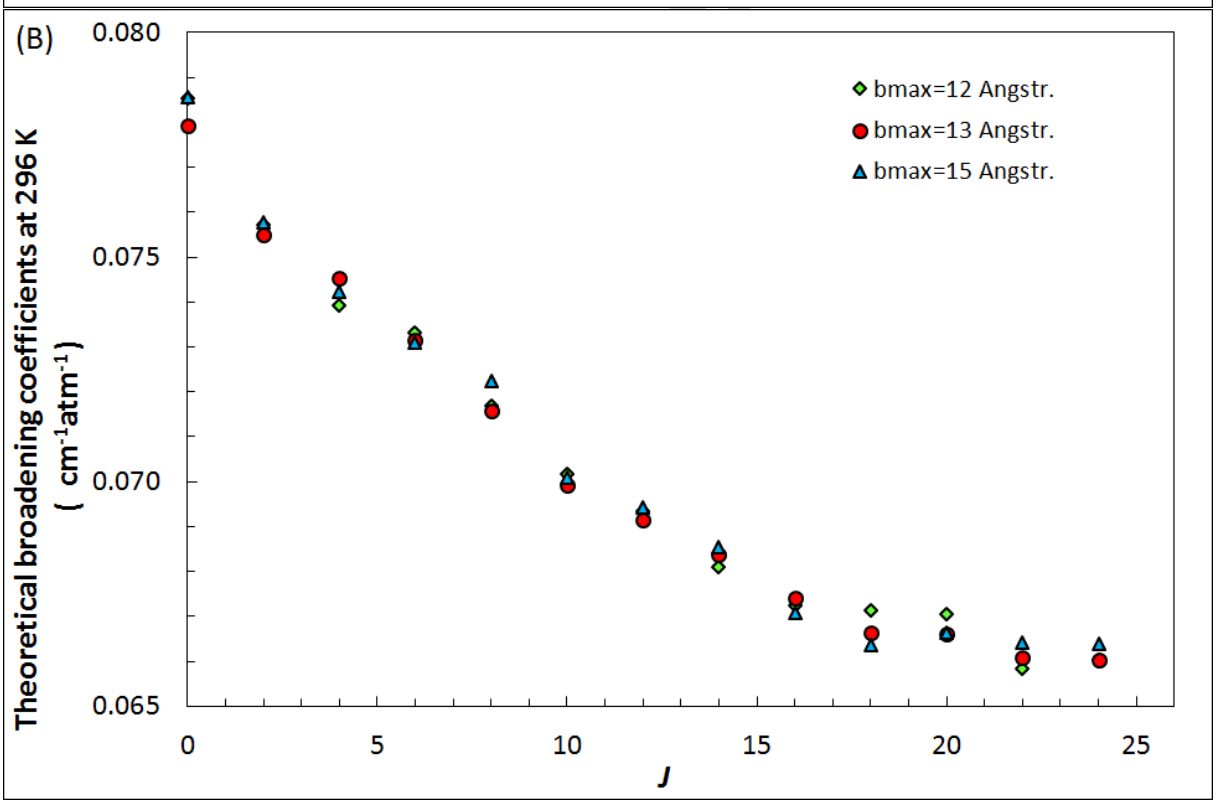

(A)
Speed Dependence Parameters
0.16
0.14
0.12
0.10
0.08
0.06
0.04
0.02
-26
-22
-18
-14
-10
-6
-2
2
6
10
14
18
22
26
m
Devi et al. 2012, SD-Voigt
SD-Voigt
Kochanov 2017

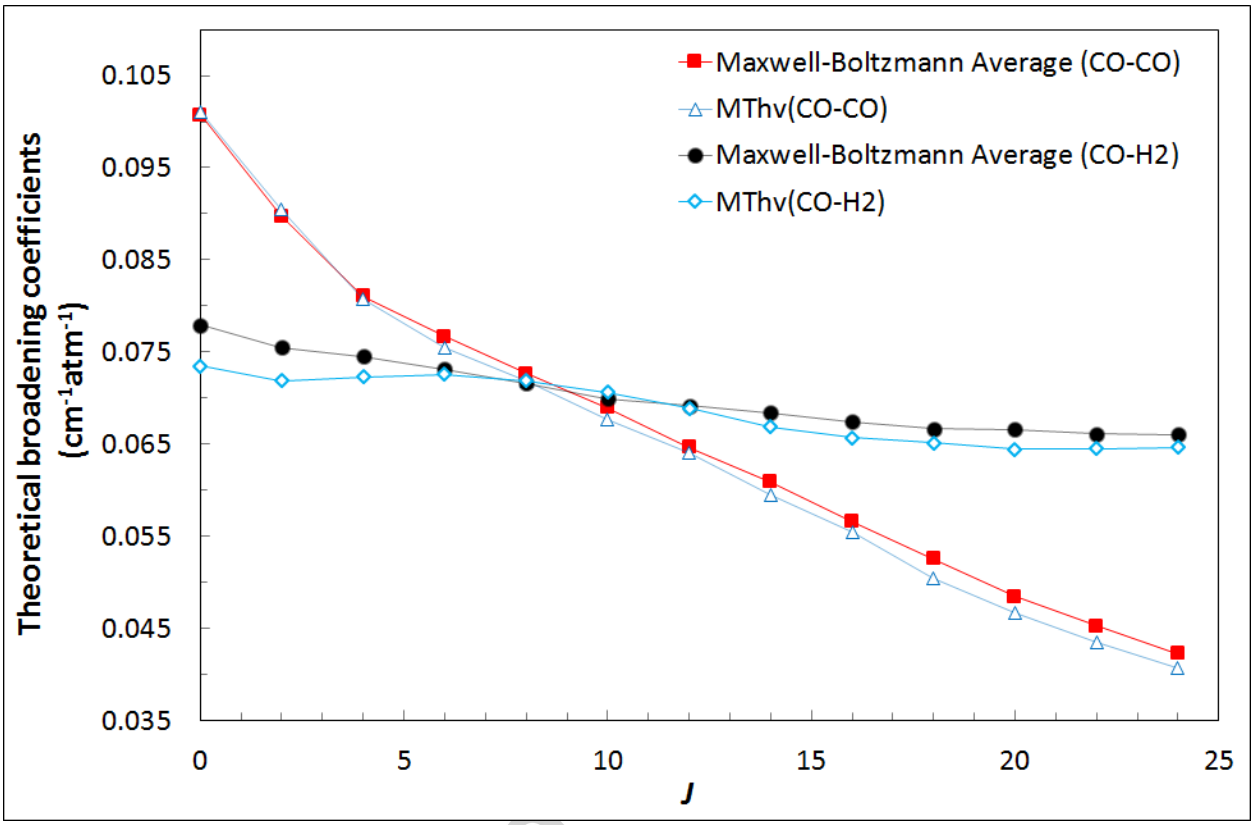
Accepted



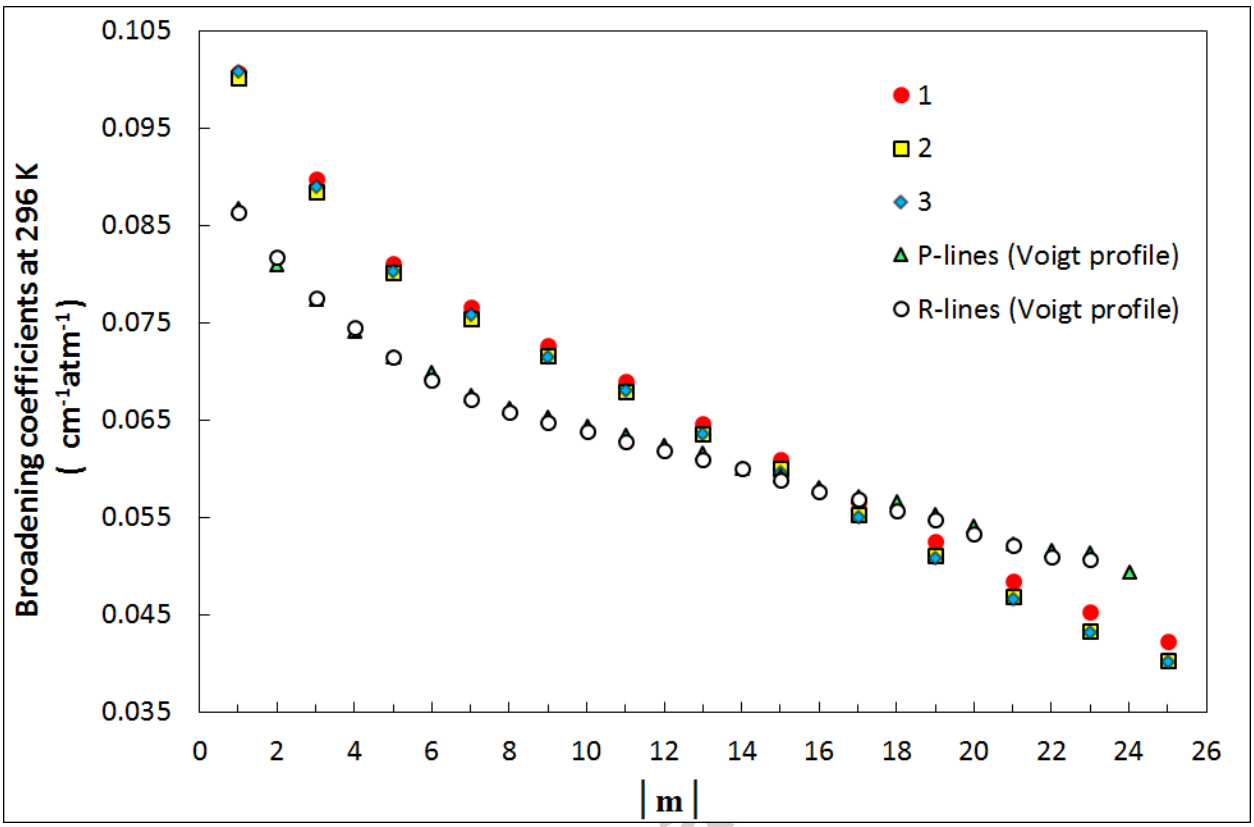
Accepted manuscript


(A)
Theoretical broadening coefficients at 296 K
(cm-1atm-1)
0.11
0.09
0.07
0.05
0.03
0
5
10
15
20
25
J
bmax=14 Angstr.
bmax=19 Angstr.
bmax=25 Angstr.

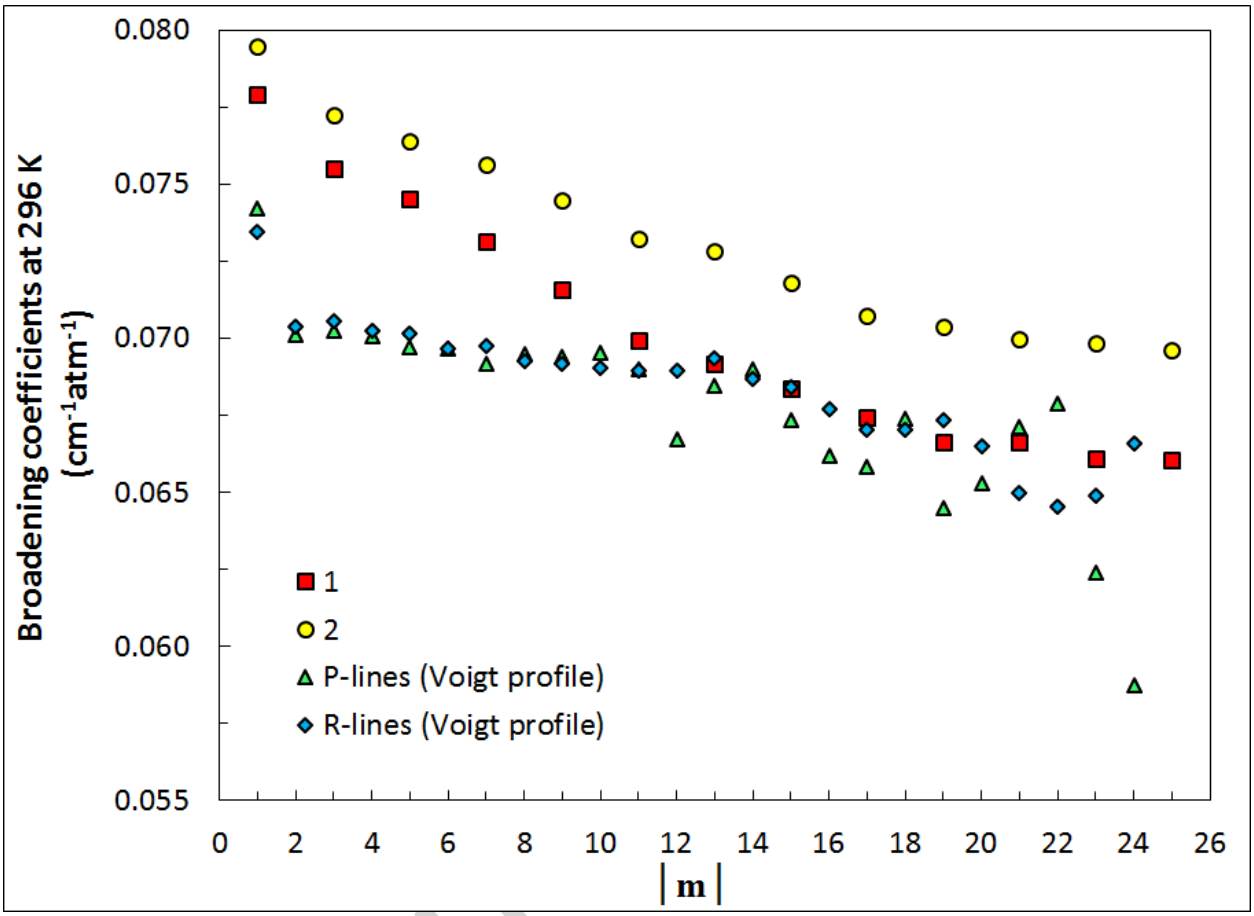

(B)
Theoretical broadening coefficients at 296 K
(cm-1atm-1)
0.080
0.075
0.070
0.065
0
5
10
15
20
25
J
bmax=12 Angstr.
bmax=13 Angstr.
bmax=15 Angstr.


Maxwell-Boltzmann Average (CO-CO)
MThv(CO-CO)
Maxwell-Boltzmann Average (CO-H2)
MThv(CO-H2)
Theoretical broadening coefficients (cm-1atm-1)
0.105
0.095
0.085
0.075
0.065
0.055
0.045
0.035
0
5
10
15
20
25
J

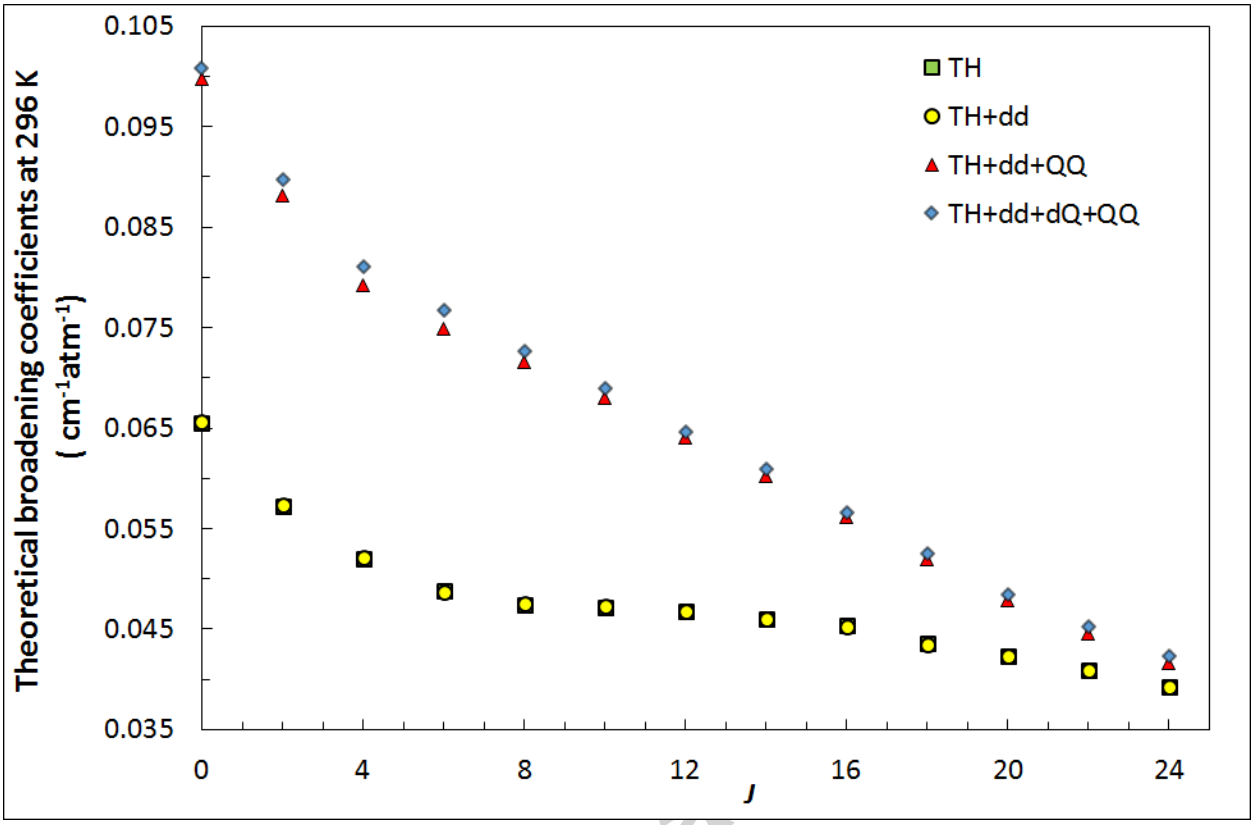
Accepted


Broadening coefficients at 296 K
(cm-1atm-1)
0.105
0.095
0.085
0.075
0.065
0.055
0.045
0.035
0
2
4
6
8
10
12
14
16
18
20
22
24
26
| m |
1
2
3
P-lines (Voigt profile)
R-lines (Voigt profile)

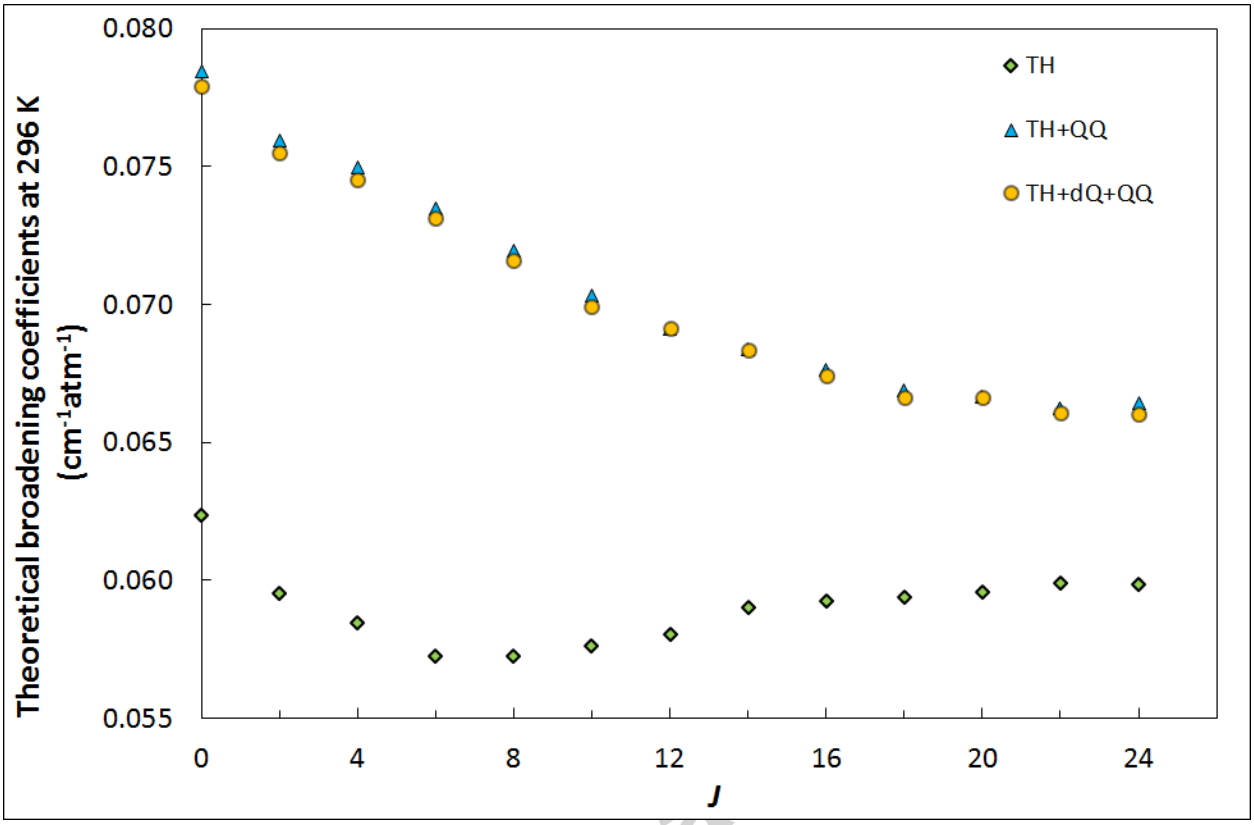
Accepted ma


Broadening coefficients at 296 K
(cm-1atm-1)
0.080
0.075
0.070
0.065
0.060
0.055
0
2
4
6
8
10
12
14
16
18
20
22
24
26
| m |
1
2
P-lines (Voigt profile)
R-lines (Voigt profile)

Accepted


Theoretical broadening coefficients at 296 K
(cm-1atm-1)
0.105
0.095
0.085
0.075
0.065
0.055
0.045
0.035
0
4
8
12
16
20
24
J
TH
TH+dd
TH+dd+QQ
TH+dd+dQ+QQ

Accepted ma


Theoretical broadening coefficients at 296 K
(cm-1atm-1)
0.080
0.075
0.070
0.065
0.060
0.055
0
4
8
12
16
20
24
J
TH
TH+QQ
TH+dQ+QQ

Accepted ma